Received: 12 February 2023 | Revised: 14 June 2023 | Accepted: 15 June 2023

DOI: 10.1002/cac2.12470

CANCER COMMUNICATIONS Open Access

ORIGINAL ARTICLE

An HGF-dependent positive feedback loop between bladder cancer cells and fibroblasts mediates lymphangiogenesis and lymphatic metastasis

Yuting Li[1,†] | **Hanhao Zheng**[2,3,†] | **Yuming Luo**[4,†] | **Yan Lin**[2,3,†] | **Mingjie An**[2,3] | **Yao Kong**[4] | **Yue Zhao**[5] | **Yina Yin**[1] | **Le Ai**[1] | **Jian Huang**[2,3] | **Changhao Chen**[2,3]

[1]Department of Oncology, Sun Yat-sen Memorial Hospital, Guangzhou, Guangdong, P. R. China

[2]Cancer Center, Renmin Hospital of Wuhan University, Wuhan, Hubei, P. R. China

[3]Department of Urology, Sun Yat-sen Memorial Hospital, Sun Yat-sen University, Guangzhou, Guangdong, P. R. China

[4]Guangdong Provincial Key Laboratory of Malignant Tumor Epigenetics and Gene Regulation, Sun Yat-sen Memorial Hospital, State Key Laboratory of Oncology in South China, Guangzhou, Guangdong, P. R. China

[5]Department of General Surgery, Guangdong Provincial People's Hospital, Guangdong Academy of Medical Sciences, Guangzhou, Guangdong, P. R. China

Correspondence
Changhao Chen, M.D., Ph.D. Department of Urology, Sun Yat-sen Memorial Hospital, 107 Yanjiangxi Road, Yuexiu District, Guangzhou, Guangdong 510120, P. R. China.
Email: chenchh53@mail.sysu.edu.cn

Abstract

Background: Cancer-associated fibroblasts (CAFs) play a vital role in facilitating tumor progression through extensive reciprocal interplay with cancer cells. Tumor-derived extracellular vesicles (EVs) are the critical mediators involved in the crosstalk between cancer cells and stromal cells, contributing to the

Abbreviations: CAFs, Cancer-associated fibroblasts; EVs, extracellular vesicles; LN, lymph node; BCa, bladder cancer; lncRNAs, long non-coding RNAs; PDX, patient-derived xenograft; MIBC, muscle-invasive bladder cancer; TME, tumor microenvironment; NATs, normal adjacent tissues; OS, overall survival; DFS, disease-free survival; ATCC, American Type Culture Collection; RPMI, Roswell Park Memorial Institute; MEM, minimal essential medium; HLECs, human lymphatic endothelial cells; ECM, endothelial cell medium; FBS, fetal bovine serum; CM, culture media; STR, short tandem repeat; RACE, 5' and 3' rapid amplification of cDNA ends; PCR, polymerase chain reaction; PBS, phosphate-buffered saline; α-SMA, alpha-Smooth Muscle Actin; FAP, fibroblast activation protein; PDGFRα, platelet-derived growth factor receptor-α; FSC-A, forward-scatter area; SSC-A, side-scatter area; FACS, fluorescence-activated cell sorting; DTT, dithiothreitol; ROC, receiver operating characteristic; BSA, bovine serum albumin; GFP, green fluorescent protein; IHC, immunohistochemistry; NSG, nonobese diabetic/severe combined immunodeficiency/interleukin-2r-γ-null; αHGF, neutralizing antibody against hepatocyte growth factor; FRET, fluorescence resonance energy transfer; CD, circular dichroism; TFOs, triplex-forming oligonucleotides; TTS, triplex target sites; TAMRA, tetramethyl-rhodamine; FAM, fluorescein amidite; TCGA, The Cancer Genome Atlas; GEPIA, Gene Expression Profiling Interactive Analysis; hnRNPL, heterogeneous nuclear ribonucleoprotein L; SPSS, Statistical Product and Service Solutions; SD, standard deviations; $\chi 2$ test, chi-square test; ANOVA, 1-way analysis of variance; scRNA-seq, single-cell RNA sequencing; LYVE-1, lymphatic vessel endothelial hyaluronan receptor 1; MLD, micro-lymphatic vessel density; ISH, in situ hybridization; FISH, fluorescence in situ hybridization; qRT-PCR, quantitative real-time PCR; siRNA, small interfering RNA; MS, Mass spectrometry; RIP, RNA immunoprecipitation; ChIRP, chromatin isolation by RNA purification; H3K4me3, H3K4 trimethylation; ChIP, chromatin immunoprecipitation; $LINC00665^{KO}$, LINC00665 knockout; $LINC00665^{WT}$, LINC00665 wild type; $CAFs^{LINC00665\text{-}EVs}$, LINC00665-induced EVs; IL-6, interleukin 6; IL-8, interleukin 8; Dkk-1, dickkopf WNT signaling pathway inhibitor 1; CXCL10, C-X-C motif chemokine ligand 10; VEGF, vascular endothelial growth factor; ELISA, enzyme-linked immunosorbent assay; GEO, Gene Expression Omnibus; nt, nucleotides..

[†]These authors contributed equally to this study.

Funding information
National Key Research and Development Program of China, Grant/Award Numbers: 2022YFA1305500, 2018YFA0902803; National Natural Science Foundation of China, Grant/Award Numbers: 82173272, 82173271, 81825016, 82103536, 82103416, 81871945, 81902589; Guangdong Basic and Applied Basic Research Foundation, Grant/Award Numbers: 2021B1515020091, 2020A1515010815, 2018B010109006, 2021A1515010355; Science and Technology Program of Guangzhou, China, Grant/Award Numbers: 202002030388, 201803010049, 2017B020227007

metastasis of cancers. Yet, the biological mechanisms of tumor-derived EVs in triggering CAFs phenotype to stimulate the lymph node (LN) metastasis of bladder cancer (BCa) are largely unknown. Here, we aimed to explore the effects and molecular mechanisms of tumor-derived EV-mediated CAFs phenotype in regulating BCa LN metastasis.

Methods: The high-throughput sequencing was utilized to identify the crucial long non-coding RNA (lncRNA) associated with CAF enrichment in BCa. The functional role of the transition of fibroblasts to CAFs induced by LINC00665-mediated EVs was investigated through the in vitro and in vivo assays. Chromatin isolation by RNA purification assays, fluorescence resonance energy transfer assays, cytokine profiling and patient-derived xenograft (PDX) model were performed to explore the underlying mechanism of LINC00665 in the LN metastasis of BCa.

Results: We found that CAFs are widely enriched in the tumor microenvironment of BCa, which correlated with BCa lymphangiogenesis and LN metastasis. We then identified a CAF-associated long non-coding RNA, LINC00665, which acted as a crucial mediator of CAF infiltration in BCa. Clinically, LINC00665 was associated with LN metastasis and poor prognosis in patients with BCa. Mechanistically, LINC00665 transcriptionally upregulated RAB27B expression and induced H3K4me3 modification on the promoter of RAB27B through the recruitment of hnRNPL. Moreover, RAB27B-induced EVs secretion endowed fibroblasts with the CAF phenotype, which reciprocally induced LINC00665 overexpression to form a RAB27B-HGF-c-Myc positive feedback loop, enhancing the lymphangiogenesis and LN metastasis of BCa. Importantly, we demonstrated that blocking EV-transmitted LINC00665 or HGF broke this loop and impaired BCa lymphangiogenesis in a PDX model.

Conclusion: Our study uncovers a precise mechanism that LINC00665 sustains BCa LN metastasis by inducing a RAB27B-HGF-c-Myc positive feedback loop between BCa cells and fibroblasts, suggesting that LINC00665 could be a promising therapeutic target for patients with LN metastatic BCa.

KEYWORDS
bladder cancer, Cancer-associated fibroblasts, extracellular vesicles, HGF, lymphangiogenesis, lymph node metastasis, long non-coding RNA, positive feedback loop

1 | INTRODUCTION

Bladder cancer (BCa) is one of the most common urinary malignancies, with an estimated 550,000 newly diagnosed cases worldwide yearly [1]. Intensive research has demonstrated that muscle-invasive bladder cancer (MIBC) possesses a particularly tumorigenic microenvironment to acquire a higher incidence of lymph node (LN) metastasis, contributing to the poor prognosis of patients [2, 3]. Cisplatin-based neoadjuvant therapy combined with radical cystectomy is determined as the standard treatment for patients with advanced BCa, which hardly improved the 5-year survival rate of patients with LN metastasis [4]. Thus, elucidating the precise mechanism triggering BCa LN metastasis and developing new therapeutic strategies for patients with LN metastatic BCa is of great clinical importance.

Lymphangiogenesis refers to the sprouting of lymphatic vasculature in the microenvironment, which enlarges the lymphatic draining system for disseminating cancer cells [5, 6]. We and others have demonstrated that regulatory signals from the tumor microenvironment (TME) are

essential for lymphangiogenesis and positively associated with increased LN metastasis and poor prognosis of patients [7–9]. However, the predominant mediators in TME that trigger lymphangiogenesis are largely unknown. Cancer-associated fibroblasts (CAFs) are the major stromal cell component in the TME that generate various cytokines to shape the desmoplastic microenvironment, leading to tumor therapeutic resistance [10]. Moreover, CAFs deliver molecular signals to cancer cells to regulate cancer cell epithelial-mesenchymal transition and maintain stemness, resulting in tumor dissemination [11, 12]. Therefore, it is of great significance to uncover the biological role and regulatory mechanisms of CAFs in mediating BCa lymphangiogenesis and LN metastasis.

Emerging evidences revealed that extracellular vesicles (EVs) serve as crucial mediators for intercellular communication and may extensively involve in the interaction profile between cancer cells and CAFs [13, 14]. Tumor cell-derived EVs specifically reshape the stromal cellular phenotype, which induces a premetastatic niche to support tumor metastasis [15]. Considering the key role of EVs in the crosstalk between tumor cells and CAFs and their advantages in biocompatibility and immunological inertness, great efforts have been made in engineered EVs for cancer therapy [16, 17]. Gene modification of the membrane surface proteins endows engineered EVs of high tissue targeting, exhibiting a significant effect in inhibiting tumor proliferation and metastasis [16, 18]. Thus, elucidating the mechanism of EVs underlying the regulation of the trafficking among tumor cells and CAFs to induce BCa lymphangiogenesis is of great clinical significance for developing effective engineered EV-dependent therapeutic method of LN metastatic BCa.

Long non-coding RNAs (lncRNAs) play a vital role in activating the signaling cascade in the TME [19, 20]. Various regulatory lncRNAs have been reported to be selectively packaged into EVs to regulate the metastatic microenvironment formation and promote tumor metastasis [21, 22]. Yet, the essential EV-associated lncRNAs mediating the CAF phenotype are largely unexplored. In this present study, we aimed to identify the crucial EV-associated lncRNAs contributed to the lymphangiogenesis and LN metastasis in BCa and explore the underlying mechanism of EV-associated lncRNAs in mediating CAF enrichment to sustain BCa LN metastasis, thus developing effective therapeutic targets for patients with LN metastatic BCa.

2 | MATERIALS AND METHODS

2.1 | Patients and clinical samples

All BCa tissues and normal adjacent tissues (**NATs**) in this study were collected from patients (containing 152 males and 76 females) who had undergone surgery at the Sun Yat-Sen Memorial Hospital of Sun Yat-Sen University (Guangzhou, Guangdong, China) and were pathologically diagnosed with BCa independently by three pathologists. The BCa patients combined with primary tumors of other systems or without complete follow-up information were excluded. The tissues underwent total RNA extraction, or formalin fixation and paraffin embedding for immunostaining. The patients were followed up regularly after surgery, in which the last date and median time of patient follow-up were 31st June 2021 and 34.7 months, respectively. Moreover, the overall survival (OS) of patients in our study was defined as the time from surgery to death, while disease-free survival (DFS) referred to the time from surgery until evidence of tumor recurrence. Our study has acquired informed consent from patients and the approval of the Sun Yat-Sen University Committees for Ethical Review of Research involving Human Subjects (approval number: 2013[61]).

2.2 | Cell lines and cell culture

The T24 (American Type Culture Collection [ATCC], Cat# HTB-4, RRID: CVCL_0554) and 5637 (ATCC, Cat# HTB-9, RRID: CVCL_0126) human BCa cell lines were purchased from American Type Culture Collection (Manassas, Virginia, USA) and were cultured in Roswell Park Memorial Institute (RPMI) 1640 medium (Invitrogen, Waltham, Massachusetts, USA, Cat# 1640TS). Fibroblasts were isolated from fresh normal urinary bladder tissues of humans and maintained in minimal essential medium (MEM; Invitrogen, Waltham, MA, USA, Cat# A1048801). Human lymphatic endothelial cells (HLECs) were obtained from ScienCell Research Laboratories (Carlsbad, California, USA, Cat# 2500) and cultured in endothelial cell medium (ECM; ScienCell Research Laboratories, Cat# 1001) supplemented with 5% fetal bovine serum (FBS). All other culture media (CM) were supplemented with 10% FBS (Gibco, Indianapolis, Indiana, USA, Cat# 10093). All cells were cultured at 37°C with 5% CO_2 in a humidified incubator, and the authentication and mycoplasma testing were qualified by short tandem repeat (STR) DNA profiling.

2.3 | 5' and 3' rapid amplification of cDNA ends (RACE) of LINC00665

Here, 5' and 3' RACE assays were performed using the 5'/3' RACE Kit (Roche, USA, Cat# 3353621001) to detect the full length of LINC00665. Briefly, the gene-specific RACE products were collected from polymerase chain reaction (PCR) amplification following separation and purification. Then, the sequence of PCR products was acquired by bidirectional sequencing. The LINC00665-specific nested PCR primer sequences are listed in Supplementary Table S1.

2.4 | Flow cytometry analysis of fibroblast phenotype

The LINC00665 EVs-induced fibroblasts with or without treatment with SIS3 were washed with phosphate-buffered saline (PBS), followed by fixation and permeabilization. They were then incubated with primary antibodies: alpha-smooth muscle actin (α-SMA, 1.137 μg/mL; Cat# ab7817, Abcam, Boston, MA, USA), fibroblast activation protein (FAP, 0.25 μL/10^6 cells; Cat# FAB3715G-100, R&D Systems, Minneapolis, USA), and platelet-derived growth factor receptor-α (PDGFRα, 1.15 μg/mL; Cat# ab203491, Abcam) at 4°C for 30 min and with the corresponding secondary fluorescent antibodies: anti-Mouse IgG (0.1μg/mL; Cat# A32773, Invitrogen, California, USA) and anti-Rabbit IgG (1μg/mL; Cat# A32731, Invitrogen, California, USA) at 4°C for another 30 min. Subsequently, the treated cells were analyzed using a FACScan flow cytometer (Becton Dickinson, Brea, California, USA). Data analysis was performed using FlowJo (Version 10, TreeStar, Ashland, Oregon, USA). Cells were first gated based on the forward-scatter area (FSC-A) and side-scatter area (SSC-A) scatters to exclude debris. Single cells were selected based on FSC-W versus FSC-H parameters, which was recommended in Becton Dickinson BioScience (BD, San Jose, California, USA) fluorescence-activated cell sorting (FACS) equipment. The isotype controls for indicated primary antibodies were used for gating, and the cell samples were then examined with indicated antibodies for further validation of the gating. The gating strategy for flow cytometry analysis is shown in Supplementary Figure S1.

2.5 | Western blotting analysis

The RIPA lysis buffer and BCA Protein Assay Kit (Thermo Fisher Scientific, Cat# 23227) were used to extract the total proteins and determine the concentration, respectively. Then, the total proteins were subjected to western blotting analysis to detect the expression of indicated proteins. After separating in 10% SDS polyacrylamide gels (SDS-PAGE), the proteins were transferred to a polyvinylidene fluoride membrane and blocked with 5% BSA for 1 h at room temperature. Then, the membrane was incubated with primary antibodies at 4°C overnight, followed by the incubation with corresponding HRP-conjugated secondary antibodies for 1 h at room temperature. The visualization of the indicated proteins was conducted using ECL reagents. The full uncut original pictures are shown in Supplementary Figure S2. The antibodies used in this study are listed in Supplementary Table S2.

2.6 | Isolation and purification of EVs

As for the isolation of urinary EVs, 50 mL mid-stream urine from patients or healthy volunteers was collected and centrifuged at 2,000 × g for 20 min followed by 10,000 × g for 30 min. Then, the obtained supernatant was filtered through a 0.22 μm filter (PALL, New York, USA) followed by ultracentrifugation at 120,000 × g for 70 min in a 70Ti rotor (Beckman, California, USA). The supernatant was discarded, and pellets were resuspended with PBS. To eliminate the Tamm-Horsfall protein, 200 mg/mL dithiothreitol (DTT) was added into the suspension and heated at 95°C for 2 min to denature the zona pellucida domains in the Tamm-Horsfall protein, after which the suspension was ultra-centrifuged at 120,000 × g for another 70 min. Finally, the pellets were resuspended with 50 μL PBS and frozen at 80°C for further use. All the centrifugations were conducted at 4°C. The receiver operating characteristic (ROC) curves were used to evaluate the efficiency of urinary EV-mediated LINC00665 in diagnosing BCa and LN metastasis

As for the isolation of EVs from the cell CM, the CM after 48 h incubation with EV-depleted FBS was collected and centrifuged sequentially at 2,000 ×g for 10 min, 10,000 ×g for 30 min, and 120,000 ×g for 70 min. Then, the pellets were rinsed in PBS through centrifugation at 120,000 ×g for 70 min and resuspended in PBS. The purified EVs were stored at -80°C for further use.

2.7 | EVs Internalization

Following the manufacturer's instruction, EVs were stained with PKH67 Green Fluorescent Cell Linker Kit (Sigma Aldrich, St Louis, USA, Cat#MINI67) and then terminated by adding 1% bovine serum albumin (BSA). PKH67-labeled EVs pellets were collected by ultracentrifugation and resuspended in an FBS-depleted medium. Then, EVs were co-cultured with fibroblasts, macrophages, T cells or B cells for 12 h. After washing

twice with PBS, cells were fixed with 4% formaldehyde and stained with DAPI. The images were obtained using a Zeiss confocal microscope system (LSM710, Zeiss, Pleasanton, CA, USA).

2.8 | Measurement of LINC00665-induced EVs on LN metastasis of BCa cells

All experimental procedures were performed with the approval of the Sun Yat-Sen University Institutional Animal Care and Use Committee (SYSEC-KY—KS-2021-293). Here, we used nude mice (4-6 weeks old, 18-20 g) purchased from the Sun Yat-Sen University Experimental Animal Center (Guangzhou, Guangdong, China). As for the mice popliteal lymphatic metastasis model, T24 cells labeled with a green fluorescent protein (GFP) were implanted into the footpads of the mice, which were then randomly divided into different groups ($n = 12$), followed by intratumoral co-injection with EVs secreted by the T24 cells. LN metastasis was detected using a PerkinElmer IVIS Spectrum In Vivo Imaging System (Xenogen Corporation, Alameda, California, USA) and analyzed when the tumors reached the same size in different groups. Immunohistochemistry (IHC) was used to analyze CAF infiltration in primary tumors.

As for the orthotopic xenograft model, 4% chloral hydras were used to anesthetize the mice. Then, an incision was made at the pubic symphysis level in the lower abdomen to expose the urinary bladder, and 5×10^5 cells resuspended in 50 μL of the medium were inoculated into the urinary bladder of mice, after which the abdomen was sutured. After the inoculation, the mice were randomly divided into three groups, followed by the treatment of indicated EVs. IHC was performed to detect the pelvic LNs.

2.9 | Establishment of mice carrying patient-derived xenografts (PDXs)

In the PDX mouse model, the 4-week-old nonobese diabetic/severe combined immunodeficiency/interleukin-2r-γ-null (NSG) mice were subcutaneously implanted with fresh BCa tissues from two patients who had undergone surgery at Sun Yat-sen Memorial Hospital of Sun Yat-sen University. When the tumors reached about 200 mm^3, the mice were randomly divided into three groups, followed by treatment with si-LINC00665 and/or neutralizing antibody against hepatocyte growth factor (αHGF). The experiments were performed with the approval of the Sun Yat-sen University Institutional Animal Care and Use Committee.

2.10 | Fluorescence resonance energy transfer (FRET) and circular dichroism (CD) spectroscopy

To determine the formation of the triplex structure between LINC00665 and the RAB27B promoter, we performed FRET and CD spectroscopy. For the FRET assays, the 5-carboxy tetramethyl-rhodamine (TAMRA) and fluorescein amidite (FAM) were labeled with triplex-forming oligonucleotides (TFOs) and triplex target sites (TTS), respectively. Then, 1:5 TFOs and TTS were mixed in binding buffer, followed by sequential incubation steps at 55°C for 10 min and 37°C for 10 h. Finally, measure the fluorescence wavelengths between 480 and 690 nm with a Molecular Device M5 Plate Reader (Molecular Device, CA, USA).

For CD spectroscopy, 1:1 TFOs and TTS were mixed with a binding buffer and equilibrated at 30°C for 1 h. Then, the fluorescence wavelengths were measured with a Chirascan spectrometer. Oligos used in the FRET and CD spectroscopy are listed in Supplementary Table S3.

2.11 | Bioinformatic analysis

The clinical significance of LINC00665 in human cancers was analyzed through The Cancer Genome Atlas (TCGA, RRID:SCR_003193) database at Gene Expression Profiling Interactive Analysis (GEPIA) (http://gepia.cancer-pku.cn/index.html, RRID:SCR_018294). The potential TFOs and corresponding TTS in LINC00665 and the promoter of RAB27B were predicted by LongTarget (http://www.gaemons.net), a lncRNA-DNA binding motif prediction tool. The secondary structures of LINC00665 and the heterogeneous nuclear ribonucleoprotein L (hnRNPL) binding motif were predicted in RNAalifold (http://rna.tbi.univie.ac.at/cgi-bin/RNAWebSuite/RNAalifold.cgi) and POSTAR3 (http://postar.ncrnalab.org/), respectively.

2.12 | Statistical analysis

All statistical analyses were conducted using Statistical Product and Service Solutions (SPSS) 13 (SPSS Inc., Chicago, IL, USA, RRID:SCR_002865) from at least three independent experiments, in which $P < 0.05$ was considered statistically significant. Quantitative data were presented as the means ± standard deviations (SD). The statistical significance of nonparametric variables was assessed by the chi-square test (χ^2 test). Parametric variables were analyzed with the 2-tailed Student's t test or 1-way analysis of variance (ANOVA). The patients'

OS and DFS were analyzed with the Kaplan-Meier method.

3 | RESULTS

3.1 | LINC00665 is correlated with CAF-induced LN metastasis of BCa

The characteristics and interactions of cancer cells and interstitial cells within the TME determine cancer invasiveness and promote cancer metastasis, which changes dynamically as cancers develop [23]. Thus, to evaluate the infiltrated cellular characteristics essential for BCa invasiveness, we re-analyzed the previous single-cell RNA sequencing (scRNA-seq) results [14] to show that CAFs were the most infiltrated cells in invasive BCa tissues (n = 4) compared with non-invasive BCa (n = 4) (Figure 1A-E), indicating that CAFs may contribute to the invasiveness of BCa. To map the CAFs enriched in BCa TME, we then evaluated the differentially expressed genes in CAFs and revealed that α-SMA, FAP and PDGFRα were highly enriched in these infiltrated CAFs (Figure 1F-I). IHC analysis in 228-case BCa cohort revealed a higher infiltration of CAFs in the mucosal layer of invasive BCa tissues than in non-invasive BCa tissues (Supplementary Figure S3A-B). Previous studies demonstrated that the activation of cancer invasiveness stimulates cancer cell metastasis preferentially to sentinel LNs, which predicts the poor OS of patients with BCa [24]. Therefore, we hypothesized that CAF infiltration might be involved in BCa LN metastasis. To confirm this hypothesis, the immunofluorescent staining assays in a large cohort of 228 BCa cases were conducted, which showed that the infiltration of CAFs was significantly increased in LN metastatic BCa tissues compared with those without LN metastasis (Figure 1J). Strikingly, a positive correlation between CAF infiltration and lymphatic vessel endothelial hyaluronan receptor 1 (LYVE-1) indicated micro-lymphatic vessel density (MLD) in BCa tissues (Figure 1J), suggesting that substantial CAF infiltration in TME plays an important role in the lymphangiogenesis and LN metastasis of BCa.

Previous studies have demonstrated that lncRNAs in tumor-induced EVs are crucial in mediating the TME to promote tumor LN metastasis [9, 25]. Thus, we explored the lncRNA expression profile in urinary EVs from five BCa patients and five healthy participants (GEO: GSE156308) and identified the crucial EV-associated lncRNAs involved in BCa LN metastasis. As shown in Figure 1K, 255 lncRNAs were upregulated more than twofold in EVs from BCa patients compared with those from healthy controls, which were then integrated with the overexpressed lncRNAs in BCa tissues compared with paired NATs as well as in LN-positive compared with LN-negative BCa (GEO: GSE106534). The results showed that 12 lncRNAs were consistently overexpressed in EVs from BCa patients than controls and in LN-positive BCa tissues than LN-negative [26]. Further evaluation in our 228-case BCa cohort demonstrated that LINC00665 was markedly overexpressed in BCa tissues compared with NATs (Figure 1L). Consistently, analysis of the TCGA database demonstrated that LINC00665 was overexpressed in various human cancers and was associated with the poor prognosis of patients (Figure 1M, Supplementary Figure S3C–P). LINC00665 was overexpressed in LN-positive (n = 53) compared with LN-negative BCa tissues (n = 175) in the whole cohort of patients and gender subgroup (Figure 1N, Supplementary Figure S3Q–R and Supplementary Table S4). Metastatic LNs had higher LINC00665 expression levels than in the primary tumor (Figure 1O). In situ hybridization (ISH) further revealed a higher LINC00665 expression in tissues from LN metastatic BCa than those from BCa without LN metastasis (Figure 1P), indicating that LINC00665 is widely contributed to the LN metastasis of BCa. Moreover, higher LINC00665 expression was related to shorter OS and DFS of both total patients and female subgroup patients (Figure 1Q and R, Supplementary Figure S3S-T). Univariate and multivariate Cox analysis showed that LINC00665 was an independent prognostic factor for OS and DFS of BCa patients (Supplementary Table S5 and S6). Importantly, we found that LINC00665 overexpression was presented with a higher CAF infiltration and around MLD in both the intratumoral and peritumoral regions of BCa tissues (Figure 1S-T, Supplementary Figure S4A-D), suggesting that LINC00665 is contributed to CAF-induced LN metastasis of BCa.

3.2 | LINC00665 enhances EV production to promote the transition of fibroblasts into CAFs

Strikingly, a higher extracellular expression level of LINC00665 was observed in LN metastatic BCa tissues than those without LN metastasis through ISH and fluorescence in situ hybridization (FISH) analysis (Figure 1P, Supplementary Figure S4E), indicating that LINC00665 might involve in BCa LN metastasis via an extracellular manner. A previous study proposed that as nanoscale vesicles widely distributed in stromal matrix, EVs could carry abnormally expressed lncRNAs to play an essential role in cell-to-cell communication [27]. Therefore, we determined whether LINC00665 exerted its function in BCa LN metastasis via EVs. Firstly, quantitative real-time PCR (qRT-PCR) analysis revealed that LINC00665 was slightly upregulated in less invasive BCa cell lines

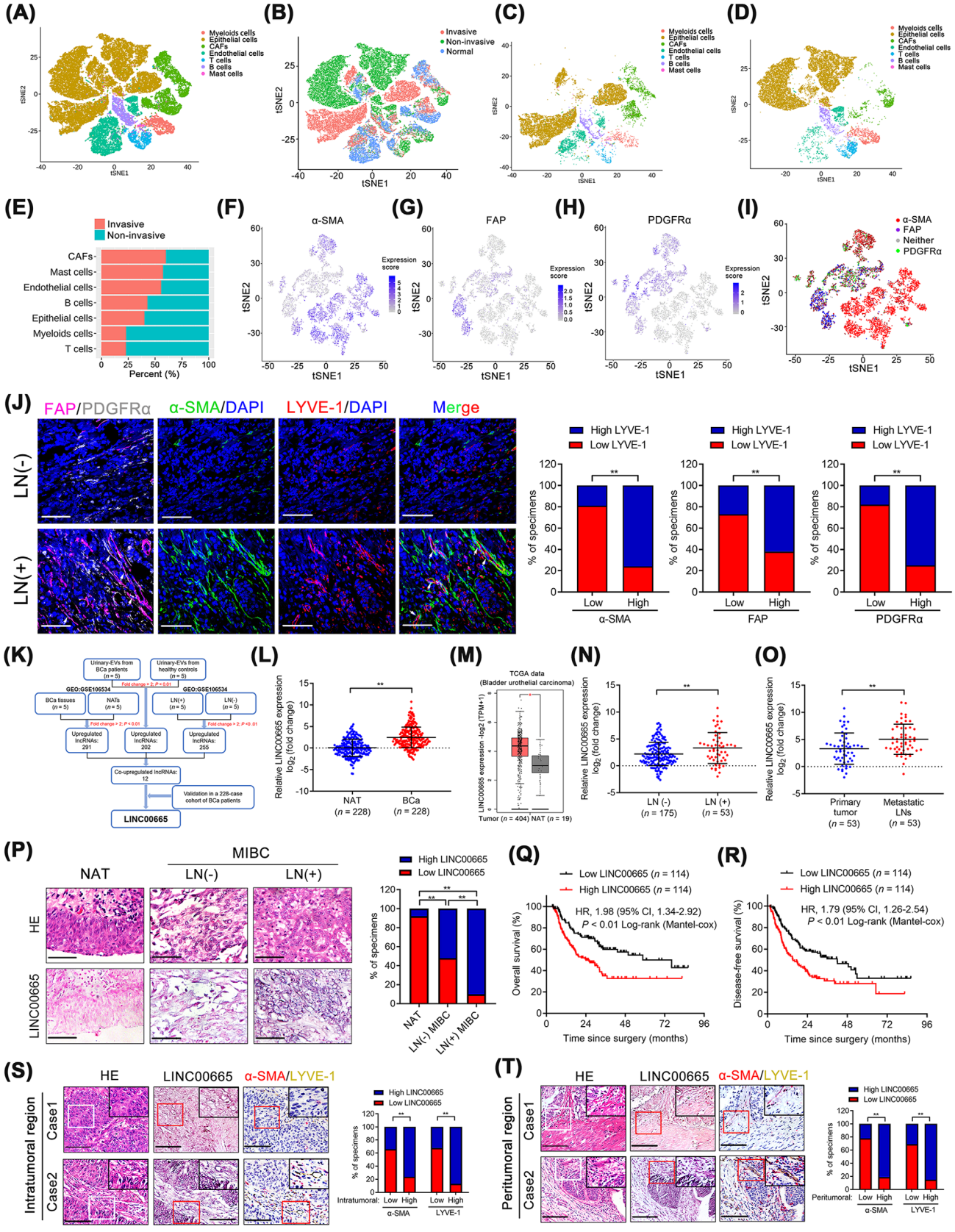

and significantly upregulated in those with high invasive compared to the SV-HUC-1 (Supplementary Figure S4F). Then, the LINC00665 expression was successfully upregulated by transfecting with LINC00665 overexpressing plasmids and downregulated by LINC00665-targeted small interfering RNA (siRNA) transfection in BCa cells (Supplementary Figure S4G-N). Then, the CM was collected to isolate the BCa cell-secreted EVs. The results indicated that LINC00665 overexpression markedly increased EV secretion in BCa cells compared with the control (Figure 2A-C, Supplementary Figure S4O-S). Since tumor-derived EVs were mainly internalized by stromal cells in TME to affect the biological activity of stromal cells, we then evaluated the recipient cells of EVs induced by LINC00665 overexpression in the BCa microenvironment. The results showed that PKH67-labelled LINC00665 overexpression-induced EVs were mostly internalized by primary fibroblasts rather than other stromal cells in the TME of BCa (Figure 2D). Considering that the extracellular molecular signals from cancer cells possessed a significant role in mediating the phenotypic features of stromal cells [28], we further investigated the role of BCa cell-secreted EVs induced by LINC00665 overexpression on the phenotype of fibroblasts. Incubating with LINC00665-overexpressing BCa cell-secreted EVs dramatically increased α-SMA, FAP and PDGFRα expression levels in fibroblasts compared with the control, while the EV-free soluble fraction from LINC00665-overexpressing BCa cells showed rare effects in α-SMA, FAP and PDGFRα expression levels in fibroblasts compared with the control (Figure 2E-G, Supplementary Figure S4T-W). Reversely, silencing LINC00665 significantly impaired the promoted effect of BCa cell-secreted EVs in CAF phenotypic proteins expression in fibroblasts (Supplementary Figure S4X and Y), suggesting that LINC00665-induced EVs promote the transition of fibroblast to CAF phenotype. Collectively, these data reveal that LINC00665 overexpression enhances the EV secretion of BCa cells to endow fibroblasts with CAF phenotype.

3.3 | LINC00665 promotes CAF infiltration to mediate BCa lymphangiogenesis and LN metastasis in vitro and in vivo

To evaluate the biological function of fibroblasts pretreated with LINC00665-induced EVs, tube formation and Transwell assays in HLECs were performed. Overexpressing LINC00665 triggered BCa cell-secreted EV-treated fibroblasts to induce the tube formation and migration of HLECs compared with the control, whereas knockdown of LINC00665 possessed the opposite effect (Figure 2H-I, Supplementary Figure S5A), indicating that LINC00665-mediated transition of fibroblasts to CAFs stimulates lymphangiogenesis of BCa in vitro. Next, a previously reported popliteal LN metastasis model in nude mice was established to evaluate the function of LINC00665-induced CAF infiltration on the lymphangiogenesis and LN metastasis of BCa in vivo [25, 29]. Firstly, equal volumes of CM from BCa cells were collected, and the EVs were isolated and verified by NTA assays to be intratumorally injected into the primary footpad tumor of mice (Figure 3A-B). The results indicated that the LINC00665-induced EVs significantly facilitated GFP-labeled T24 cell metastasis to the popliteal LNs compared to the control EVs (Figure 3C-D,

FIGURE 1 LINC00665 is correlated with CAF-induced LN metastasis of BCa. (A) tSNE plot of single cells identified by scRNA-seq and colored by major cell types. (B) tSNE plot of single cells identified by scRNA-seq and colored by tissue types. (C) tSNE plot of single cells identified by scRNA-seq and colored by major cell types in non-invasive BCa tissues. (D) tSNE plot of single cells identified by scRNA-seq and colored by major cell types in invasive BCa tissues. (E) The fraction of major cell types profiled from non-invasive and invasive BCa tissues. (F-H) tSNE plot showed the expression of (F) α-SMA, (G) FAP, and (H) PDGFRα on CAFs. (I) Gene overlays of indicated CAF markers on tSNE. (J) Representative images and percentages revealing a positive correlation between α-SMA, FAP and PDGFRα-indicated CAF infiltration and LYVE-1-indicated lymphatic vessel density in BCa tissues ($n = 228$). Scale bar: 50 μm. (K) Flowchart showing the identification of lncRNAs upregulated in both urinary EVs and LN-positive tissues from BCa patients. (L and M) Evaluating LINC00665 expression in BCa tissues and NATs in a 228-case cohort (L) and TCGA database (M). (N and O) Evaluating LINC00665 expression in BCa tissues with or without LN metastasis (N) and in primary BCa tissues and paired metastatic LNs (O). (P) Representative ISH images and percentages of LINC00665 expression (blue) in NATs, LN-negative BCa tissues and LN-positive BCa tissues. Scale bar: 50 μm. (Q and R) Kaplan-Meier curves for OS (Q) or DFS (R) of BCa patients ($n = 228$) according to LINC00665 expression. The cutoff value is the median expression. (S and T) Representative images and percentages of CAF enrichment and MLD in the intratumoral (S) and peritumoral regions (T) of BCa tissues ($n = 228$). White or red squares represent the areas of the insets. Scale bar: 50 μm. Statistical significance was assessed by the χ^2 test in J, P, S and T, or the nonparametric Mann-Whitney U test in L-O. *$P < 0.05$, **$P < 0.01$. *Abbreviations*: CAFs, Cancer-associated fibroblasts; LN, lymph node; BCa, bladder cancer; tSNE, T-distributed stochastic neighbor embedding; scRNA-seq, single-cell RNA sequencing; α-SMA, alpha-Smooth Muscle Actin; FAP, fibroblast activation protein; PDGFRα, platelet-derived growth factor receptor-α; LYVE-1, lymphatic vessel endothelial hyaluronan receptor 1; EVs, extracellular vesicles; lncRNAs, long non-coding RNAs; NATs, normal adjacent tissues; TCGA, The Cancer Genome Atlas; OS, overall survival; DFS, disease-free survival; MLD, micro-lymphatic vessel density.

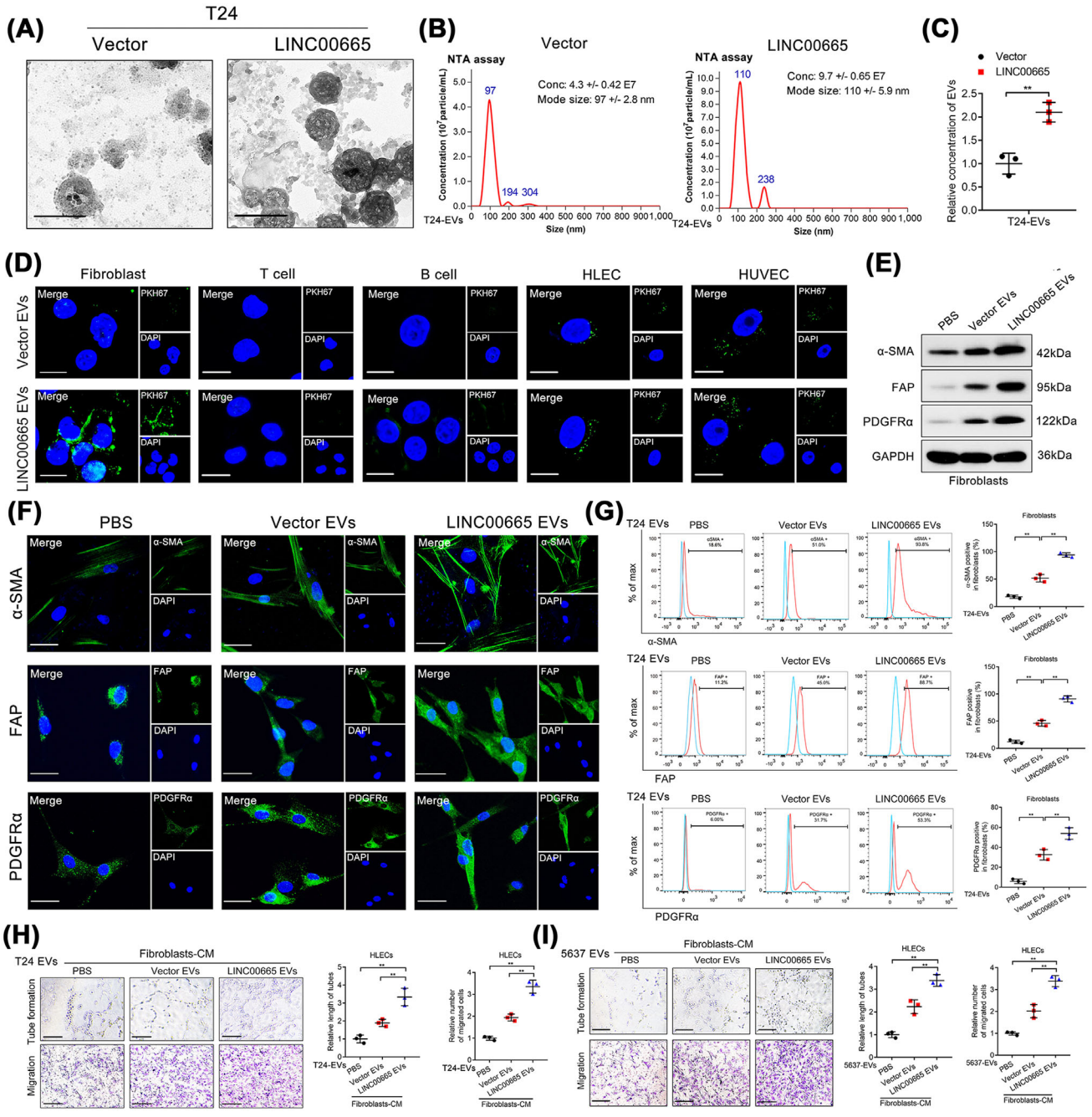

FIGURE 2 LINC00665-induced EVs endow fibroblasts with CAF phenotype to promote BCa lymphangiogenesis in vitro. (A) Representative TEM images of EVs isolated from LINC00665-overexpressing T24 and control cells. Scale bars: 100 nm. (B and C) NTA analysis and quantification of EVs isolated from T24 cells with or without transiently transfecting with the Vector or LINC00665-overexpressing plasmids. (D) Representative fluorescence images of primary fibroblasts, T cells, B cells, HLECs and HUVECs after incubation with PKH67-labelled (green) vector EVs or LINC00665 EVs from BCa cells. Scale bars: 5 μm. (E) Western blotting analysis of α-SMA, FAP and PDGFRα expression in fibroblasts incubated with PBS, vector- or LINC00665-induced EVs from BCa cells. (F) Representative confocal images of α-SMA, FAP and PDGFRα expression in fibroblasts treated with PBS, vector- or LINC00665-induced EVs from BCa cells. Scale bars: 5 μm. (G) Flow cytometric analysis of α-SMA, FAP and PDGFRα expression in fibroblasts incubated with PBS, vector-induced EVs, or LINC00665-induced EVs form BCa cells. (H and I) Representative images and quantification of tube formation and Transwell migration of HLECs incubated with CM from fibroblasts treated with PBS, vector-induced EV, or LINC00665-induced EV. Scale bar: 100 μm. Statistical significance was assessed by the two-tailed Student's t test in C, or 1-way ANOVA followed by Dunnett's tests in G-I. Error bars show the SD from three independent experiments. *$P < 0.05$; **$P < 0.01$. *Abbreviations*: EVs, extracellular vesicles; CAFs, Cancer-associated fibroblasts; BCa, bladder cancer; TEM, transmission electron microscopy; NTA, nanoparticle tracking analysis; α-SMA, alpha-Smooth Muscle Actin; FAP, fibroblast activation protein; PDGFRα, platelet-derived growth factor receptor-α; PBS, phosphate-buffered saline; HLECs, human lymphatic endothelial cells; CM, culture media.

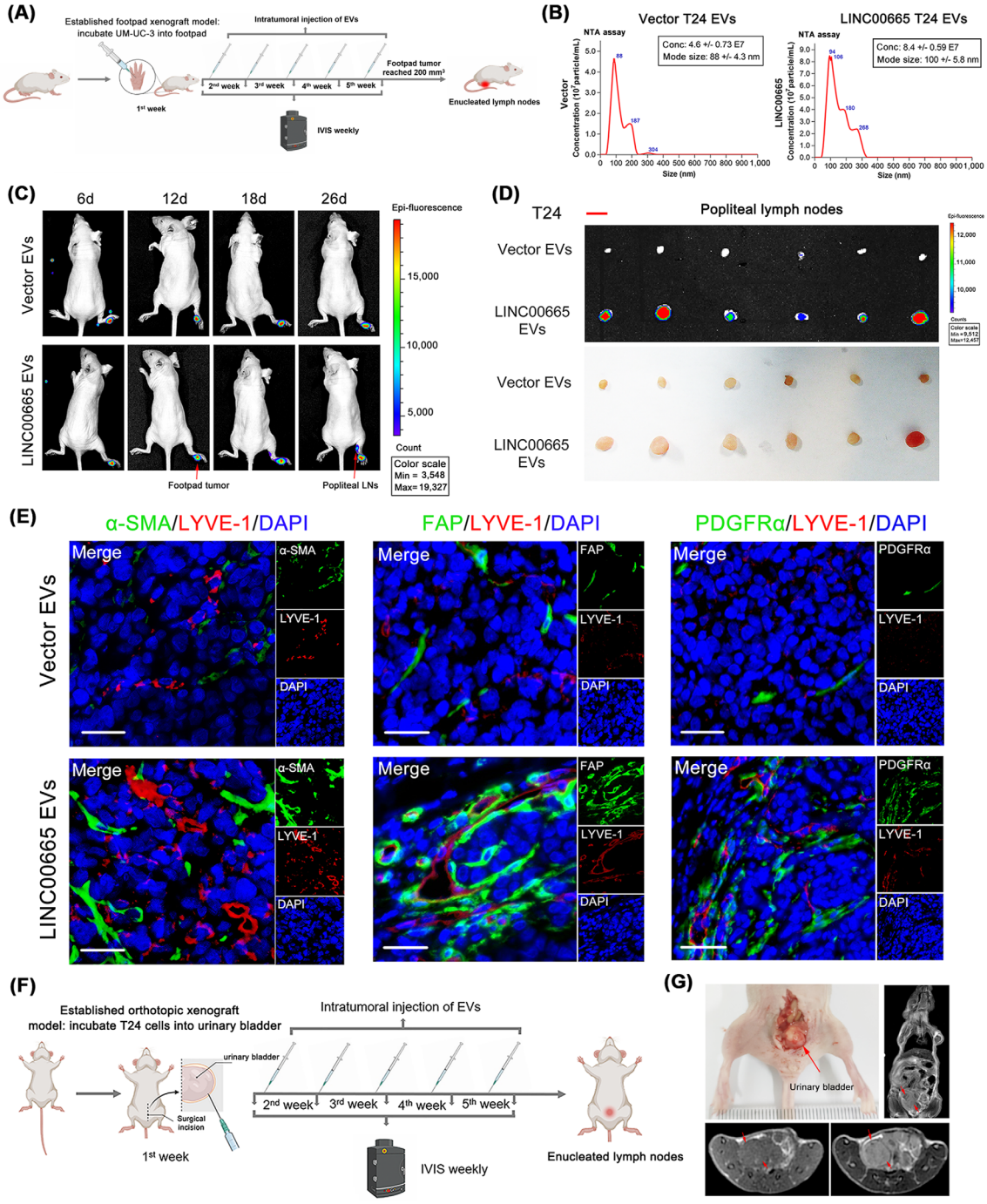

Supplementary Figure S5B-C). The metastatic rate of popliteal LNs was higher in mice treated with LINC00665-induced EVs than the control EVs (Supplementary Figure S5D-F), confirming that LINC00665-induced EVs promote the LN metastasis of BCa. Furthermore, compared with the control group, treatment with LINC00665-induced EVs significantly increased α-SMA, FAP and PDGFRα-indicated CAF enrichment around the interstitial tissues of popliteal LNs (Supplementary Figure S5G-L), confirming that the fibroblasts internalize LINC00665-induced EVs to acquire the CAF phenotype. The CAF infiltration and LYVE-1-indicated MLD were consistently increased in the LINC00665-induced EV group than the control group (Figure 3E, Supplementary Figure S5M-P), confirming that the LINC00665-induced EVs promote BCa lymphangiogenesis by stimulating CAF infiltration in vivo.

To better simulate the anatomy and physiology of LN metastasis of BCa in vivo, we used the orthotopic xenograft model to confirm the effect of LINC00665-induced EVs in the LN metastasis of BCa. T24 cells labeled with GFP were implanted into the urinary bladder of nude mice by intertumoral injection of Vector EVs or LINC00665 EVs (Figure 3F). The results showed that treatment with LINC00665-induced EVs significantly promoted the metastasis of BCa cells to LNs around the urinary bladder (Figure 3G-H). Given that the pelvic LNs around the common iliac, external iliac, internal iliac and obturator are the most frequent drainage LNs of BCa in mice, we further enucleated these LNs to investigate the LN status. The results revealed that treating with the LINC00665-induced EVs significantly promoted the pelvic LN metastasis of BCa (Figure 3I and J). Collectively, these results demonstrate that LINC00665 triggers the EV secretion from BCa cells to promote CAF infiltration and facilitate the lymphangiogenesis and LN metastasis of BCa.

3.4 | LINC00665 directly binds with hnRNPL

We further explored the molecular mechanism of LINC00665 in mediating the infiltration of CAFs and LN metastasis of BCa. The RACE assays revealed that LINC00665 was a lncRNA with a full length of 2,856 nucleotides (nt) in BCa cells (Supplementary Figure S6A-D). LINC00665 was located in both the cytoplasm and nucleus of BCa cells, but mainly in the cytoplasm (Supplementary Figure S6E-F). Subsequently, RNA pull-down assay revealed an obviously different band at 55-70 kDa in the biotinylated LINC00665 group compared with the control group, which was further confirmed as hnRNPL through Mass spectrometry (MS) and western blotting analysis (Figure 4A-D, Supplementary Figure S7A-G). Confocal fluorescence microscopy analysis validated the partial colocalization of LINC00665 and hnRNPL in the nucleus of T24 and 5637 cells (Figure 4E). RNA immunoprecipitation (RIP) assays further verified the significant enrichment of LINC00665 by hnRNPL (Supplementary Figure S7H), demonstrating the binding between LINC00665 and hnRNPL.

Next, we demonstrated that the 2,250-2,400 nt region of LINC00665 was essential for its interaction with hnRNPL (Figure 4F-G, Supplementary Figure S7I). Moreover, POSTAR3, a database for exploring the RNA-binding motif of proteins [30], was used to predict a potential binding motif of hnRNPL, which was located in the 2,285-2,360 nt region of LINC00665 and formed a stem-loop structure (Figure 4H). Deletion of the 2,285-2,360 nt region in LINC00665 significantly impaired the ability of hnRNPL to enrich LINC00665 (Figure 4I). Together, these results demonstrate that hnRNPL directly interacts with the 2,285-2,360 nt region in LINC00665.

FIGURE 3 LINC00665-induced EVs promote CAF infiltration to stimulate the LN metastasis of BCa in vivo. (A) Flowchart showing the establishment of the popliteal LN metastasis model. (B) NTA analysis of EVs isolated from T24 cells with or without infecting with the Vector or LINC00665-overexpressing lentiviruses. (C) Representative bioluminescence images of nude mice treated with vector- or LINC00665-induced EVs ($n = 12$). The red arrows indicate footpad primary tumor and metastatic popliteal LN. (D) Representative images of the popliteal LNs from mice ($n = 12$). (E) Representative images of fluorescence of α-SMA-, FAP- and PDGFRα-indicated CAF and LYVE-1-indicated lymphatic vessel density in footpad tumor from the mice ($n = 12$). Scale bar: 50 μm. (F) Flowchart showing the establishment of BCa orthotopic xenograft model. (G) Necropsy examination and MRI of mouse urinary bladders following post-inoculation. (H) Representative bioluminescence images of nude mice treated with vector- EVs or LINC00665-induced EVs ($n = 12$). The red arrows indicate primary BCa and metastatic LNs. (I) Representative images of anti-GFP analysis in pelvic LNs from the indicated group ($n = 12$). Scale bars: 500 μm (red) or 100 μm (black). (J) Quantification of the metastatic number of pelvic LNs in mice from indicated groups. Statistical significance was assessed by two-tailed Student's *t* test in J. Error bars show the SD from three independent experiments. $^{*}P < 0.05$; $^{**}P < 0.01$. *Abbreviations*: EVs, extracellular vesicles; CAFs, Cancer-associated fibroblasts; LN, lymph node; BCa, bladder cancer; NTA, nanoparticle tracking analysis; α-SMA, alpha-Smooth Muscle Actin; FAP, fibroblast activation protein; PDGFRα, platelet-derived growth factor receptor-α; LYVE-1, lymphatic vessel endothelial hyaluronan receptor 1; MRI, Magnetic resonance imaging; GFP, green fluorescent protein.

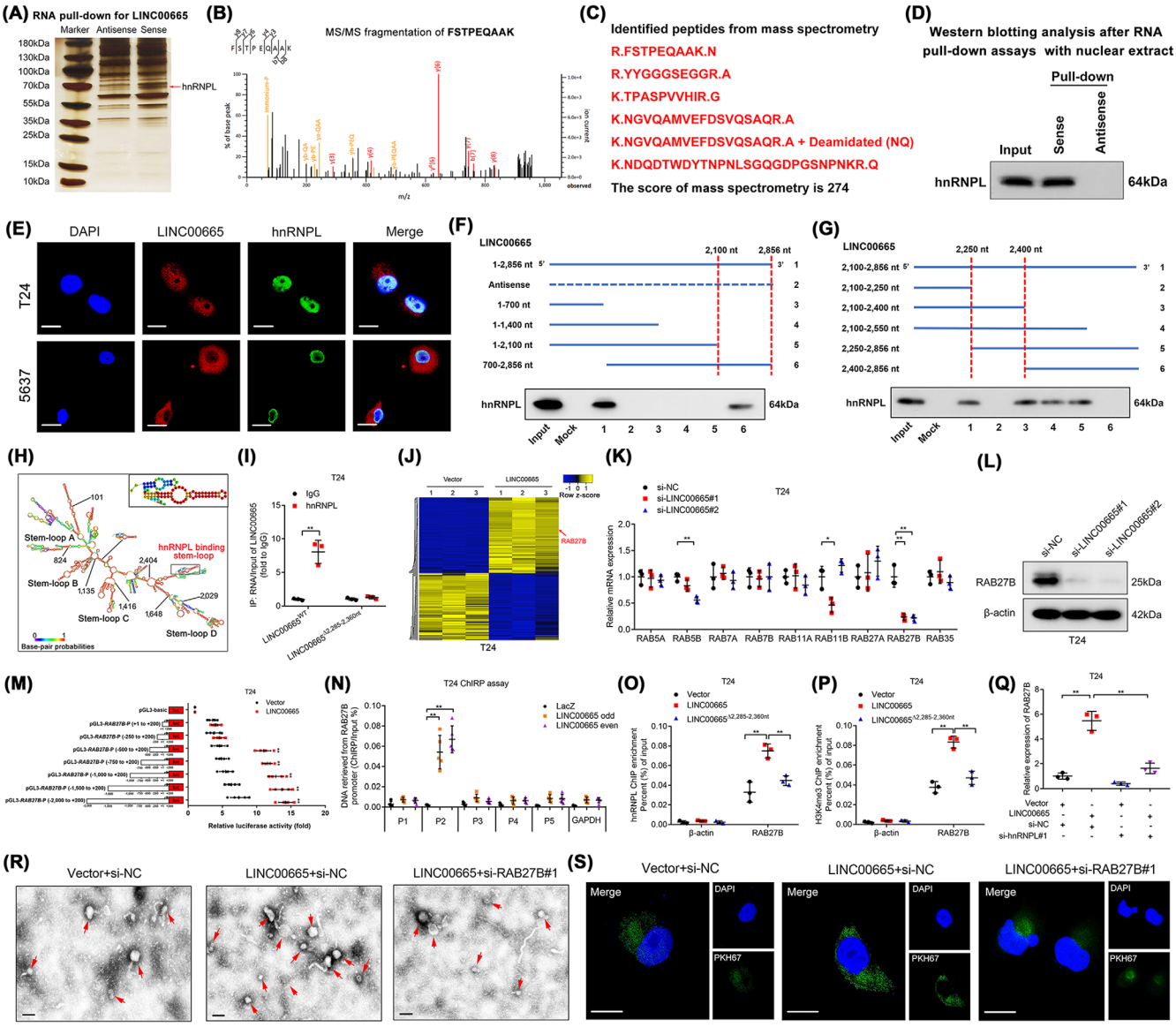

FIGURE 4 LINC00665 directly binds with hnRNPL to promote RAB27B transcription. (A-C) Silver staining of the proteins from RNA pull-down assays performed by biotin-labeled LINC00665 sense and antisense in T24 cells, and MS analysis of the LINC00665-enriched band from silver staining. (D) Western blotting analysis after RNA pull-down assays with nuclear extract. (E) Relative fluorescence showing the colocalization of LINC00665 and hnRNPL in the nucleus of T24 and 5637 cells. Scale bar: 5 μm. (F and G) RNA pull-down with serial deletions of LINC00665 identified the essential regions on LINC00665 required for binding hnRNPL (Vertical red lines). Horizontal blue lines showed the full-length or serial deletions of LINC00665. (H) RNAalifold for predicting the stem-loop structures of the hnRNPL binding sites in LINC00665. (I) RIP assays after deletion of 2285-2360 nt region of LINC00665 in T24 cells. (J) Heatmap of the differentially expressed genes between LINC00665-overexpressing and control BCa cells. (K) qRT-PCR analysis of the change in RAB genes related to EV secretion after silencing LINC00665 in T24 cells. (L) Western blotting analysis of RAB27B expression after LINC00665 silencing in T24 cells. (M) Luciferase analysis with serial deletion of RAB27B promoter in T24 cells with or without overexpressing LINC00665. (N) Ten probes of LINC00665 numbered 1 to 10 were divided into the odd group (LINC00665 odd) and even group (LINC00665 even). LINC00665-enriched chromatin in T24 cells was revealed by ChIRP analysis. (O and P) ChIP analysis of the hnRNPL enrichment and H3K4me3 status of the RAB27B promoter in LINC00665-overexpressing T24 cells with or without muting of the hnRNPL binding site. (Q) qRT-PCR analysis of RAB27B expression in LINC00665-overexpressing T24 cells with or without hnRNPL silencing. (R) Representative TEM of EVs secreted by vector- or LINC00665 plasmid-transfected T24 cells with or without RAB27B silencing. Red arrows indicate the EVs. Scale bar: 100 nm. (S) Representative immunofluorescence images of fibroblasts treated with PKH67-labelled EVs secreted by indicated BCa cells. Scale bar: 5 μm. Statistical significance was assessed by the two-tailed Student's t test in I and M, or 1-way ANOVA followed by Dunnett's tests in K and N-Q. Error bars show the SD from three independent experiments. *P< 0.05; **P < 0.01. *Abbreviations*: hnRNPL, heterogeneous nuclear ribonucleoprotein L; MS, Mass spectrometry; RIP, RNA immunoprecipitation; nt, nucleotides; qRT-PCR, quantitative real-time PCR; ChIP, chromatin immunoprecipitation; TEM, transmission electron microscopy.

3.5 | LINC00665 forms a DNA–RNA triplex structure with RAB27B promoter to promote RAB27B transcription

To profile the target genes of LINC00665, RNA sequencing was performed in LINC00665-overexpressing BCa cells and the control cells. The results showed that 542 genes were significantly overexpressed by more than two-fold in LINC00665-overexpressing BCa cells than the control (GEO: GSE190650) (Figure 4J). Since LINC00665 plays an essential role in the release of EVs from BCa cells, we further analyzed the change of Ras-related Rab protein family expression associated with EV secretion (Figure 4K, Supplementary Figure S8A and Table S7). As shown in Figure 4L and Supplementary Figure S8B–F, the results showed that RAB27B was the most significantly upregulated gene after overexpressing LINC00665, while the RAB27B expression was downregulated by knocking down LINC00665 in BCa cells. To explore the potential mechanism of LINC00665 in regulating the transcriptional activation of RAB27B, the truncated RAB27B promoter sequences (-2,000 to +200 bp) were cloned into the pGL3 luciferase plasmids and subjected to luciferase assays. We found that overexpressing LINC00665 markedly increased the transcriptional activity of the -250 to -500 bp sequence in the RAB27B promoter (Figure 4M, Supplementary Figure S8G). Subsequently, chromatin isolation by RNA purification (ChIRP) assays verified that LINC00665 physiologically interacted with the P2 region (-315 to -327 bp) in the promoter of RAB27B (Figure 4N, Supplementary Figure S8H-I). Furthermore, the potential TFOs and corresponding TTS in LINC00665 and the promoter of RAB27B were predicted. Then, these TFOs and TTS were labeled with TAMRA and FAM, respectively. As shown in Supplementary Figure S8J, an obvious positive peak at 270-280 nm and a negative peak at 210 nm in the LINC00665 TFO2/RAB27B TTS2 group were revealed by CD spectroscopy, consistent with the results from the FENDRR/PITX2 positive control [31]. Moreover, FRET analysis revealed the fluorescence intensity at 570-580 nm was significantly increased and at 520 nm was decreased in the LINC00665 TFO2/RAB27B TTS2 group compared to the control group (Supplementary Figure S8K), indicating LINC00665 interacts with RAB27B promoter to form a triplex structure.

It has been demonstrated that hnRNPL was a key mediator in inducing H3K4 trimethylation (H3K4me3) to regulate the transcriptional activation of the target gene [32]. Thus, we investigated whether LINC00665 activated RAB27B transcription by recruiting hnRNPL to catalyze H3K4me3 at the promoter of RAB27B in BCa cells. The results of chromatin immunoprecipitation (ChIP) assay showed that the enrichment of hnRNPL and H3K4me3 at the RAB27B promoter was significantly increased by overexpressing LINC00665, which was attenuated by muting the hnRNPL-binding region on LINC00665 (Figure 4O-P, Supplementary Figure S8L-M). Conversely, downregulating LINC00665 significantly decreased hnRNPL and H3K4me3 enrichment at the RAB27B promoter (Supplementary Figure S8N-Q). Moreover, silencing hnRNPL significantly impaired the ability of LINC00665 to upregulate RAB27B expression (Figure 4Q, Supplementary Figure S8R). Together, these results demonstrate that LINC00665 directly binds to the RAB27B promoter to form a DNA–RNA triplex and activate RAB27B transcription.

3.6 | EV-mediated LINC00665 endows fibroblasts with the CAF phenotype by activating the TGF-β pathway

Since RAB27B is crucial in enhancing the fusion of late endocytic compartments with the plasma membrane to trigger the EV secretion [33], the essential role of RAB27B in LINC00665-induced EV secretion was evaluated by detecting the amount of secreted EVs after overexpressing RAB27B. The results revealed that the EV secretion by T24 and 5637 cells was increased by overexpressing LINC00665, which was impaired by downregulating RAB27B (Figure 4R, Supplementary Figure S8S-W). Considering that RABs have been reported to serve as vital mediators in vesicle docking and fusion with recipient cells [34], we then investigated whether RAB27B was indispensable for the internalization of LINC00665-induced EVs by fibroblasts. As shown in Figure 4S and Supplementary Figure S8X, incubating with PKH67-labeled LINC00665-induced EVs markedly increased the green fluorescence signal in the cytoplasm of fibroblasts compared with the control, which was impaired by knocking down RAB27B.

EV cargos are highly relevant in their function of communicating with recipient cells to regulate a variety of biological processes [35]. Given that LINC00665 was overexpressed in BCa-secreted EVs from our results of RNA sequencing, we further evaluated whether LINC00655-induced EVs regulated the fibroblasts through the transmission of LINC00665. First, we found that the LINC00665 expression level was markedly increased in EVs secreted by BCa cells after intracellularly overexpressing LINC00665, which was reduced by downregulating RAB27B (Supplementary Figure S9A-B). Moreover, LINC00665-induced EVs dramatically increased the expression of LINC00665 in recipient fibroblasts, which was impaired by RAB27B downregulation (Supplementary Figure S9C-D), indicating that LINC00665-mediated RAB27B expression promotes the EV transmission of LINC00665 into fibroblasts.

Then, the effect of EV-packaged LINC00665 on the EV-mediated transition of fibroblasts into CAF phenotype was further evaluated. The results showed that down-regulating LINC00665 expression in fibroblasts markedly decreased α-SMA, FAP, and PDGFRα expressions induced by LINC00665-overexpressing BCa-secreted EVs (Supplementary Figure S9E-K).

To exclude the possibility that transcriptional activation of endogenous LINC00665 in fibroblasts promoted the phenotype transition, we constructed a LINC00665 knockout (LINC00665^{KO}) fibroblasts to inhibit the endogenous LINC00665 expression (Supplementary Figure S10A-B). We then investigated the effects of LINC00665-induced EVs on LINC00665 wild type (LINC00665^{WT}) and LINC00665^{KO} fibroblasts. The results showed that LINC00665-induced EVs significantly promoted the transition of LINC00665^{KO} fibroblasts to CAFs, which was consistent with results in LINC00665^{WT} fibroblasts (Supplementary Figure S10C-E), indicating that BCa cells endow the fibroblasts with CAF phenotype by transmitting EV-mediated LINC00665 to fibroblasts.

A previous report demonstrated that activation of the TGF-β signaling pathway was essential for controlling the fibroblast phenotype in TME [36]. Here, we explored whether the TGF-β signaling pathway was essential for the EV-mediated LINC00665-induced transition of fibroblasts to CAFs. The alterations of crucial proteins in the TGF-β signaling pathway were analyzed to reveal that treating with EV-mediated LINC00665 markedly increased the phosphorylation of SMAD2 and SMAD3 in fibroblasts compared with the control, while the expressions of TGF-βR1 and TGF-βR2 were not changed after treating with EV-mediated LINC00665 (Figure 5A). Conversely, incubating with EVs from LINC00665 knocked down BCa cells significantly reduced the phosphorylation of SMAD2 and SMAD3 without affecting TGF-βR1 and TGF-βR2 expression in fibroblasts (Supplementary Figure S10F), indicating that EV-mediated LINC00665 specifically promotes SMAD2 and SMAD3 phosphorylation to activate the canonical TGF-β signaling pathway in fibroblasts. Subsequently, treatments with various TGF-β signaling pathway inhibitors were conducted to validate whether TGF-β signaling pathway activation is indispensable for the EV-mediated LINC00665-induced phenotype transition of fibroblasts. A significant increase of α-SMA, FAP, and PDGFRα expression in fibroblasts treated with EVs secreted by LINC00665-overexpressing BCa cells, which was markedly attenuated only by treating with SIS3, the specific inhibitor targeting the SMAD2 and SMAD3 phosphorylation, rather than by other inhibitors targeting the non-canonical TGF-β signaling pathways (Figure 5B-H, Supplementary Figure S10G). Together, our results demonstrate that EV-mediated LINC00665 induces the SMAD2 and SMAD3 phosphorylation to endow the fibroblasts with the CAF phenotype.

3.7 | EV-mediated LINC00665 enhances lymphangiogenesis by stimulating HGF secretion in CAFs

To detect the mechanisms of CAFs activated by EV-mediated LINC00665 (CAFs$^{LINC00665\text{-}Evs}$) in promoting lymphangiogenesis, the cytokine profile of CAFs$^{LINC00665\text{-}Evs}$ was explored. As shown in Figure 5I-J, the secretions of five cytokines, including interleukin 6 (IL-6), interleukin 8 (IL-8), Dickkopf WNT signaling pathway inhibitor 1 (Dkk-1), HGF and C-X-C motif chemokine ligand 10 (CXCL10), were significantly increased, and one was decreased in CAFs$^{LINC00665\text{-}Evs}$ compared with the control. Interestingly, we found that vascular endothelial growth factor (VEGF), the crucial regulator of tumor lymphangiogenesis, was not significantly increased in CAFs$^{LINC00665\text{-}Evs}$ compared with the control, suggesting that CAFs$^{LINC00665\text{-}Evs}$ might facilitate the lymphangiogenesis and LN metastasis of BCa through a VEGF-independent manner (Figure 5I-J). Moreover, the promoted effect of EV-mediated LINC00665 in the secretions of indicated cytokines by CAFs, including IL-6, IL-8, Dkk-1, HGF and CXCL10, was further confirmed by enzyme-linked immunosorbent assay (ELISA) yielded (Figure 5K and L). Next, we performed the in vitro assays to investigate the essential cytokines involved in CAFs$^{LINC00665\text{-}Evs}$-induced lymphangiogenesis. The results revealed that treating with αHGF dramatically impaired the tube formation and migration of HLECs promoted by CAFs$^{LINC00665\text{-}Evs}$, while inhibiting other cytokines had very few effects (Figure 5M), suggesting that EV-mediated LINC00665 facilitates BCa lymphangiogenesis by stimulating HGF secretion by CAFs.

3.8 | EV-mediated LINC00665-induced RAB27B-HGF-c-Myc positive loop is indispensable to BCa LN metastasis

Accumulating evidences have shown that cancer cell-stimulated CAFs reciprocally regulate the aggressive biological behavior of cancer cells to enhance tumor metastasis [10]. Therefore, we further examined the biological effect of CAFs$^{LINC00665\text{-}Evs}$ in BCa cells. The results showed that the expression of LINC00665 in BCa cells was significantly upregulated by co-culturing with CAFs$^{LINC00665\text{-}Evs}$ (Figure 6A-C), indicating that there is a potential positive feedback loop between BCa cells and CAFs.

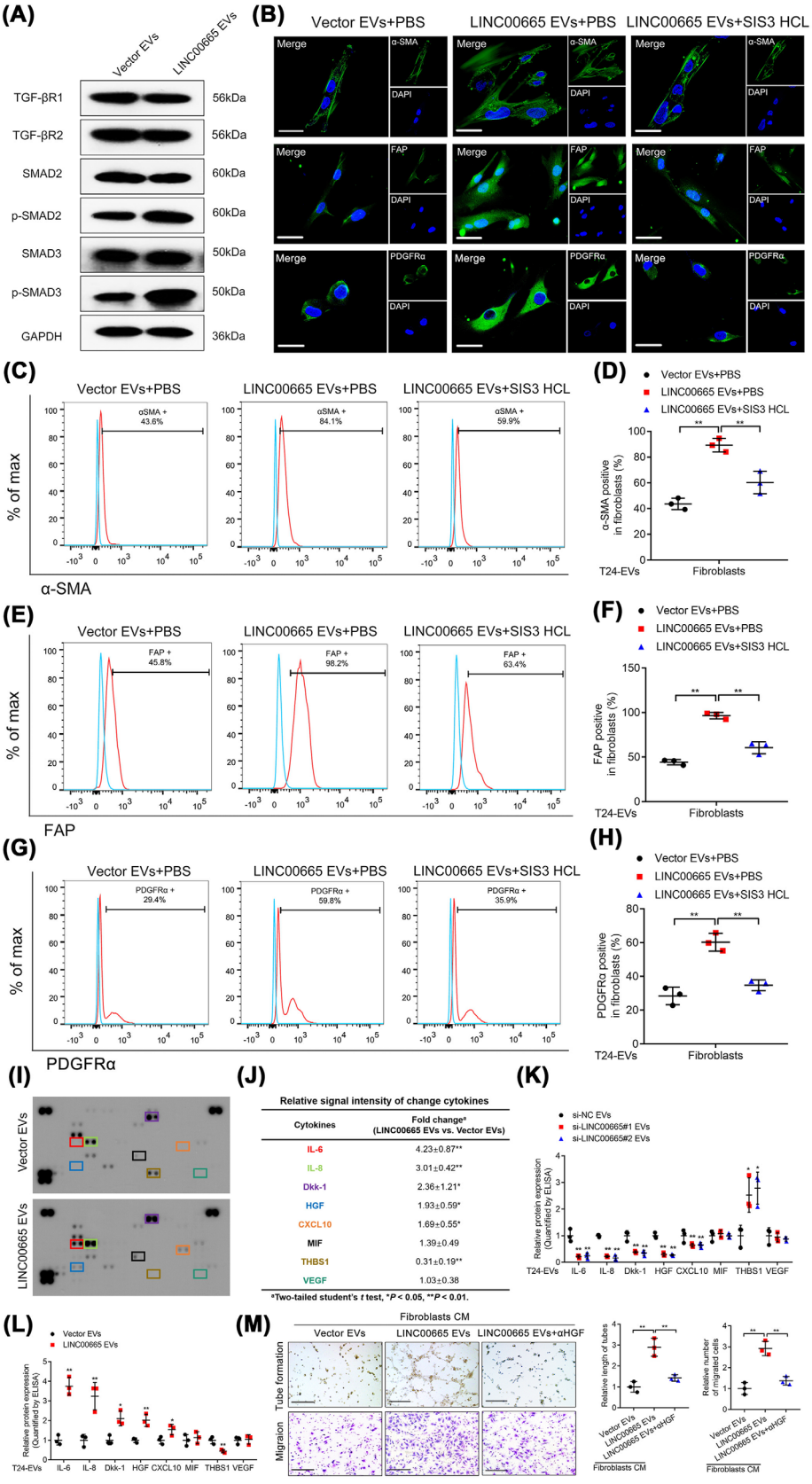

Given that CAFs could induce lncRNA transcription in cancer cells by regulating the activation of massive transcription factors [37], we evaluated the potential transcriptional factors interacting with the LINC00665 promoter that might participate in CAFs$^{LINC00665\text{-}Evs}$-upregulated LINC00665 expression. As shown in Figure 6D-F and Supplementary Figure S10H, c-Myc was the potential transcriptional factor to bind with the promoter of LINC00665, and knocking down c-Myc significantly decreased the promoted effect of HGF in the transcriptional activity of LINC00665 in BCa cells, suggesting that c-Myc is essential for LINC00665 transcription induced by CAFs$^{LINC00665\text{-}EVs}$-secreted HGF. Furthermore, ChIP analysis revealed that CAFs$^{LINC00665\text{-}EVs}$ markedly increased the enrichment of c-Myc in the -351 to -358 bp region (referred to as P2) of LINC00665 promoter rather than in another predicted binding site in -106 to -113 bp region (referred as P1) (Figure 6F-H). Mutation of the P2 region in the LINC00665 promoter significantly attenuated the promoted effect of CAFs$^{LINC00665\text{-}EVs}$ in the transcriptional activity of LINC00665, while mutating the P1 region had rare effects (Figure 6I, Supplementary Figure S10I), suggesting that CAFs$^{LINC00665\text{-}EVs}$-mediated c-Myc interacts directly with -351 to -358 bp of the LINC00665 promoter to activate its transcription.

Given that CAFs conversely activated the transcription of LINC00665, in vitro assays were performed to detect the role of the LINC00665-mediated positive feedback loop in maintaining CAF-induced lymphangiogenesis (Figure 6J). The results showed that downregulating LINC00665 expression impaired the transition of fibroblasts to CAFs triggered by incubating with BCa cells (Figure 6K-M, Supplementary Figure S10J). Moreover, treating with αHGF markedly inhibited CAF-induced LINC00665 overexpression in BCa cells and attenuated the coculturing-induced activation of CAFs (Figure 6K-M, Supplementary Figure S10J). Strikingly, either knocking down LINC00665 or treating with αHGF inhibited the fibroblast-induced tube formation and migration of HLECs in the co-culture model of BCa cells and fibroblasts (Figure 6N). Together, these results demonstrate that RAB27B-HGF-c-Myc positive feedback loop between BCa cells and fibroblasts induced by LINC00665 stimulates the lymphangiogenesis of BCa.

3.9 | Clinical relevance of the LINC00665-induced positive feedback loop in LN metastatic BCa

Since HGF plays a crucial regulatory role in LINC00665-induced positive feedback loop and BCa lymphangiogenesis, the clinical relevance of HGF in the LN metastasis of BCa was evaluated. Double immunostaining and ISH analysis revealed that higher HGF expression was presented with more CAF enrichment and MLD in LINC00665-overexpressed regions of BCa tissues (Figure 7A-C). qRT-PCR analysis showed a higher HGF and RAB27B expression in BCa tissues than the paired NATs (n = 228) (Figure 7D, Supplementary Figure S11A). The expressions of HGF and RAB27B were significantly upregulated in LN-positive BCa tissues compared with the LN-negative BCa tissues (Figure 7E, Supplementary Figure S11B-C). Moreover, HGF overexpression was associated positively with shorter OS and DFS of BCa patients (Figure 7F).

We further assessed the effect of blocking HGF in suppressing lymphangiogenesis and LN metastasis of BCa stimulated by the LINC00665-induced RAB27B–HGF–c-Myc positive feedback loop. in vitro assays showed that both fibroblasts treated with EV-mediated LINC00665 and primary CAFs dramatically promoted tube formation and migration of HLECs, while αHGF treatment dramatically abrogated these effects (Supplementary Figure S11D-I). Moreover, in vivo assays with a popliteal LN metastasis model revealed that EV-mediated LINC00665 markedly enhanced the metastasis of BCa cells to the LNs compared with the control groups, which was reversed by blocking HGF (Figure 7G). The LN metastatic rate increased by

FIGURE 5 EV-mediated LINC00665 endows fibroblasts with the CAF phenotype by activating the TGF-β pathway. (A) Western blotting analysis showing the alteration of crucial proteins of the TGF-β pathway in fibroblasts treated with EVs from LINC00665-overexpressing BCa cells. (B) Immunofluorescence analysis of α-SMA, FAP and PDGFRα expression in LINC00665-induced EV-incubated fibroblasts with or without SIS3 treatment. Scale bar: 5 μm. (C-H) Flow cytometric analysis and quantification of α-SMA (C and D), FAP (E and F) or PDGFRα (G and H) expression in LINC00665-induced EV-incubated fibroblasts with or without SIS3 treatment. (I) Cytokine array of the CM from fibroblasts treated with EVs secreted by BCa cells transfected with vector plasmids or LINC00665 plasmids. (J) The relative signal intensity of altered cytokines in the indicated group. (K and L) ELISA analysis of cytokine secretion by fibroblasts incubated with indicated EVs. (M) Representative images and quantification of tube formation and Transwell migration of HLECs treated with indicated fibroblast CM. Scale bars: 100 μm. Statistical significance was assessed by 1-way ANOVA followed by Dunnett's tests in D, F, H, K and M, or the two-tailed Student's t test in J and L. Error bars show the SD from three independent experiments. *$P < 0.05$; **$P < 0.01$. *Abbreviations*: EVs, extracellular vesicles; CAFs, Cancer-associated fibroblasts; TGF-β, transforming growth factor beta; BCa, bladder cancer; α-SMA, alpha-Smooth Muscle Actin; FAP, fibroblast activation protein; PDGFRα, platelet-derived growth factor receptor-α; CM, culture media; ELISA, enzyme-linked immunosorbent assay; HLECs, human lymphatic endothelial cells.

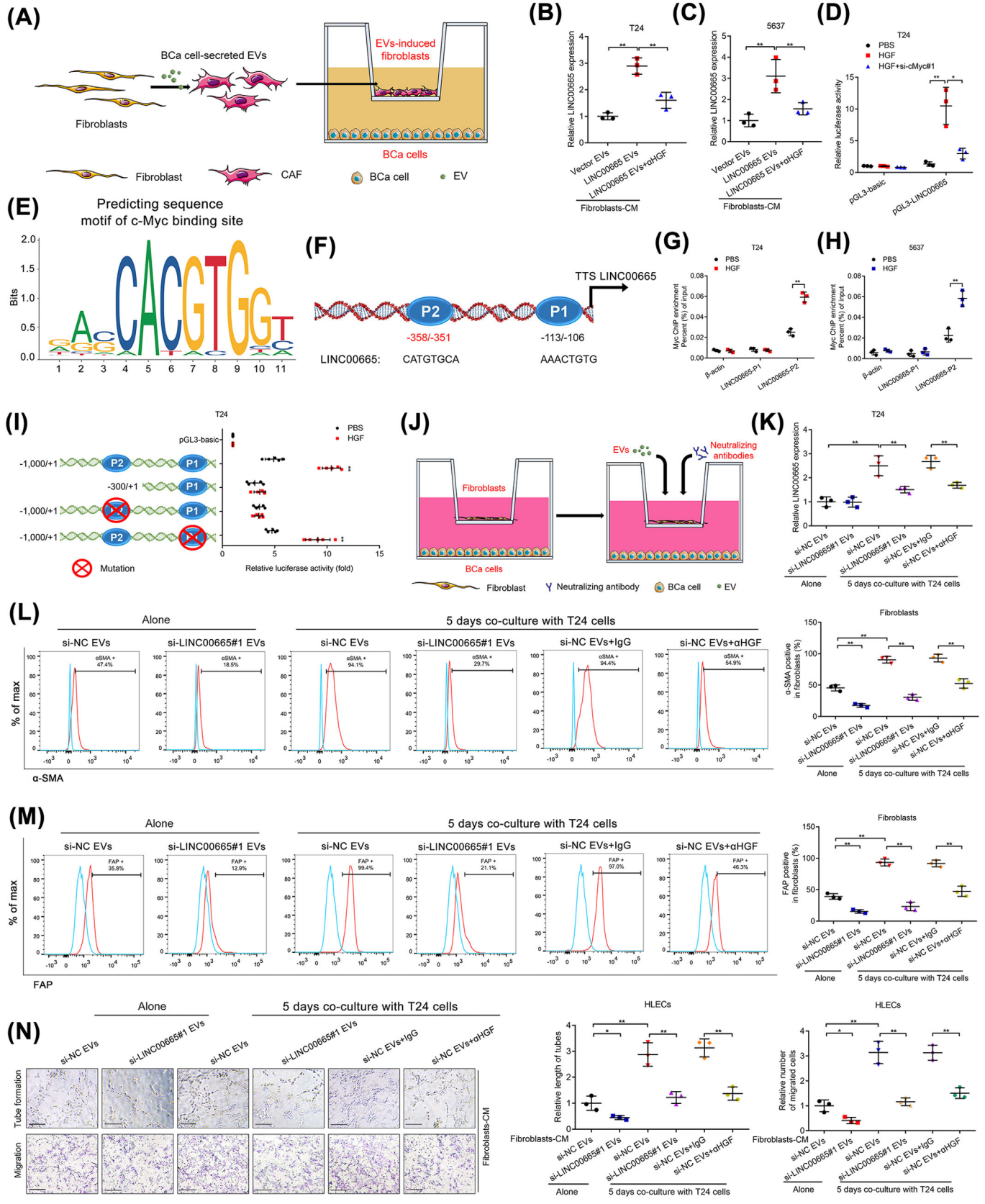

EV-mediated LINC00665 was significantly abolished by treating with αHGF (Supplementary Figure S11J). In addition, αHGF treatment markedly decreased the CAF infiltration and MLD stimulated by EV-mediated LINC00665 in the primary footpad tumor tissues (Figure 7H).

Next, we further evaluated the clinical application potential of LINC00665 and αHGF to treat LN metastatic BCa (Figure 7I). The results revealed that both decreasing LINC00665 expression and utilization of αHGF inhibited the tumor growth and prolonged the tumor-bearing survival time in the PDX model constructed with LN metastatic BCa tissues (Supplementary Figure S11K-M). Moreover, LINC00665 silencing and αHGF treatment markedly inhibited LINC00665 expression to reduce the CAF infiltration and MLD in tumor tissues in the PDX model (Figure 7J, Supplementary Figure S11N-S), implying the potential clinical application of LINC00665 and αHGF in the treatment of patients with LN metastatic BCa.

Since EV-mediated lncRNAs have emerged as encouraging early diagnostic biomarkers for cancers. Here, we evaluated the clinical relevance of EV-mediated LINC00665 in the LN metastasis of BCa. qRT-PCR analysis revealed that LINC00665 was upregulated in the urinary EVs obtained from BCa patients compared with the healthy controls (Figure 7K). Moreover, a higher expression of LINC00665 was observed in urinary EVs obtained from patients with LN metastatic BCa than those without LN metastasis (Figure 7L). Importantly, we revealed that urinary EV-mediated LINC00665 could effectively distinguish patients with BCa from healthy controls (AUC: 0.801; 95% CI: 0.76-0.84) (Figure 7M). And urinary EV-mediated LINC00665 possessed higher diagnostic accuracy in diagnosing LN metastasis in BCa than urine cytology and FISH, which were previously demonstrated as the standard non-invasive diagnostic interventions for BCa (Figure 7N). Collectively, these results suggest that EV-associated LINC00665 is a potential therapeutic target and diagnostic biomarker for LN metastatic BCa (Figure 7O).

4 | DISCUSSION

The CAF characteristics and crosstalk with other cells change dynamically as cancers evolve, in which the high enrichment of CAF marks an aggressive feature in the metastatic TME by orchestrating the invasive behavior of endothelial cells to influence tumor angiogenesis and lymphangiogenesis [38, 39]. However, the biological effects and molecular mechanisms of CAFs in mediating the lymphangiogenesis to trigger the LN metastasis of BCa remain unclear. Here, we reveal that CAFs were highly enriched in BCa TME through scRNA-seq and demonstrate that CAF infiltration was positively related to the lymphangiogenesis and LN metastasis of BCa. Moreover, we identified a CAF-associated lncRNA, LINC00665, which was found to play an important role in CAF infiltration in BCa. Mechanistically, LINC00665 transcriptionally upregulates RAB27B expression by recruiting hnRNPL to induce H3K4me3 modification on RAB27B promoter and mediates the RAB27B-dependent release of EVs to endow fibroblasts with CAF phenotype, thereby enhancing lymphangiogenesis and LN metastasis of BCa. Our findings firstly highlight the crucial role of CAFs in inducing the lymphangiogenesis to sustain BCa LN metastasis, suggesting that targeting CAF-associated lncRNA, LINC00665, to block the communication between tumor cells and fibroblasts is a promising approach to inhibit CAF infiltration and suppress the LN metastasis of BCa. Previous studies have demonstrated that CAFs possesses high functional heterogeneity in tumor progression, which were attributed to the different origin of CAFs [37]. Although we highlighted the biological effect of LINC00665 EVs-induced CAFs in LN metastasis, the roles and mechanisms of other CAF subtypes in other aspects of progression in BCa still remain unclear and need further exploration.

Previous studies have identified that HGF, a key growth factor among TME-derived signals, is critical for cancer initiation and progression [40, 41]. The sustaining

FIGURE 6 The LINC00665-mediated positive loop is indispensable for LN metastasis of BCa. (A) Schematic presentation of the established BCa cells and EV-induced fibroblasts co-culture model. (B and C) qRT-PCR analysis of LINC00665 expression in BCa cells cultured with indicated CM from fibroblasts with or without αHGF treatment. (D) Relative transcriptional activity of LINC00665 in HGF-treated T24 cells with or without c-Myc silencing. (E) Enriched motifs of c-Myc binding sites predicted by JASPAR. (F) Schematic model of c-Myc binding sequences in the LINC00665 promoter region predicted by JASPAR and PROMO. (G and H) ChIP-qPCR analysis of c-Myc-enriched chromatin in T24 (G) and 5637 (H) cells. (I) Depletion of the P1 region in the LINC00665 promoter impaired the HGF-induced LINC00665 transcriptional activity in T24 cells. (J) Schematic presentation of the co-culture model for analysis of the positive loop between BCa cells and fibroblasts. (K) qRT-PCR analysis of LINC00665 expression in T24 cells incubated with indicated fibroblasts. (L and M) Flow cytometry analysis and percentages of α-SMA (L) and FAP (M) expression of fibroblasts. (N) Representative images and quantification of tube formation and Transwell migration of indicated HLECs. Scale bar: 100 μm. Statistical significance was assessed by 1-way ANOVA followed by Dunnett's tests in B-D and K-N, or the two-tailed Student's *t* test in G-I. Error bars show the SD from three independent experiments. $^{*}P < 0.05$; $^{**}P < 0.01$. *Abbreviations*: LN, lymph node; BCa, bladder cancer; EVs, extracellular vesicles; qRT-PCR, quantitative real-time PCR; CM, culture media; αHGF, neutralizing antibody against HGF; ChIP, chromatin immunoprecipitation; qRT-PCR, quantitative real-time PCR; α-SMA, alpha-Smooth Muscle Actin; FAP, fibroblast activation protein; HLECs, human lymphatic endothelial cells.

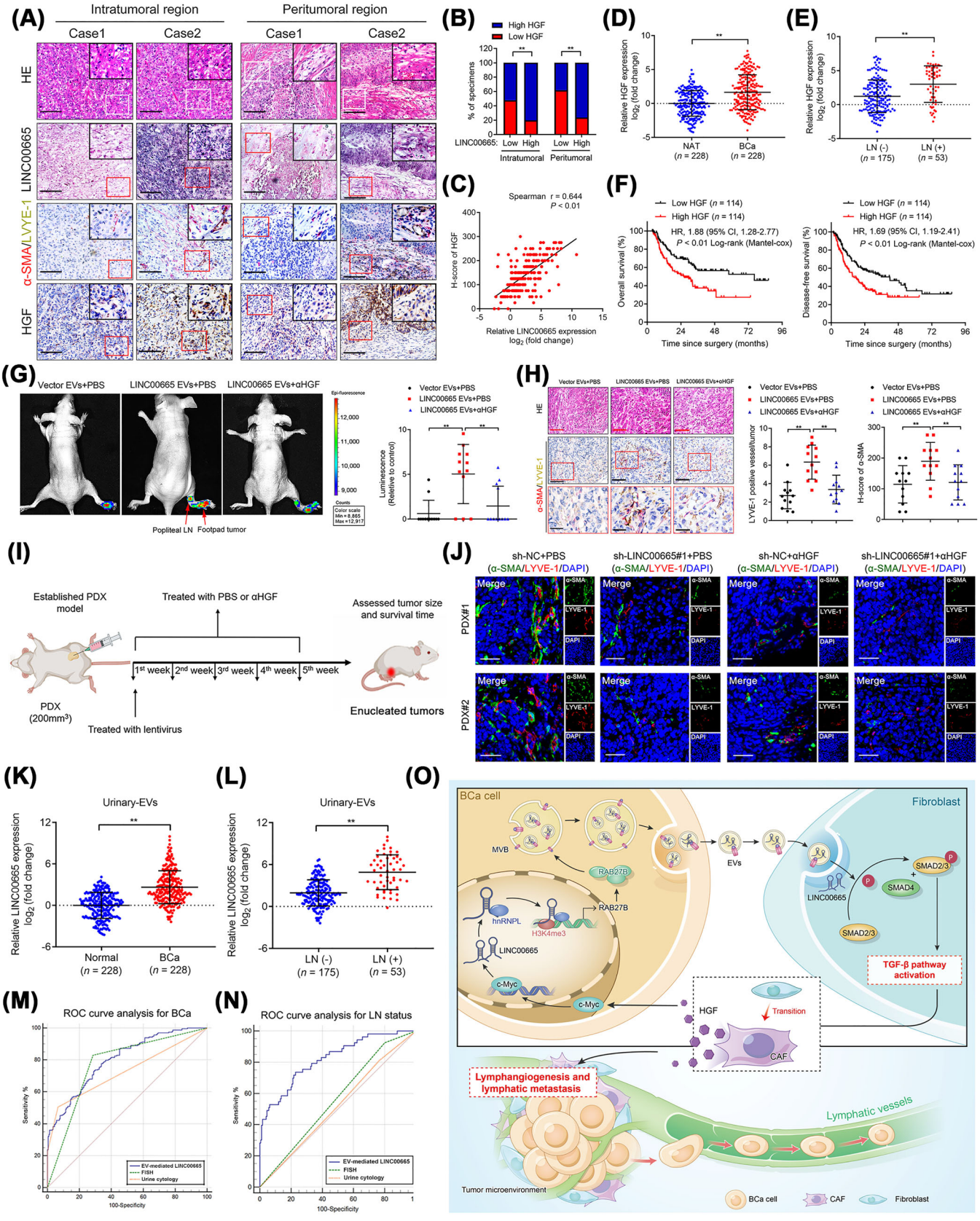

secretion of HGF stimulates the activation of downstream signaling pathways to shape the metastatic microenvironment and allow the cancer cells to acquire a metastatic mesenchymal phenotype [42]. However, the effect of targeting HGF signaling on tumor lymphangiogenesis is largely unknown. Herein, we determined that the secretion of HGF sustained by LINC00665-induced RAB27B-HGF-c-Myc positive feedback loop between cancer cells and fibroblasts was widely involved in the regulation of the lymphangiogenesis and LN metastasis of BCa. Blocking HGF exhibited a prominent effect in inhibiting BCa lymphangiogenesis and LN metastasis both in vitro and in vivo. Moreover, using PDX models with LN metastatic BCa tissues, we first reported that blocking EV-transmitted LINC00665 or HGF significantly reduced tumor burden. Our results provide preliminary evidence for targeting HGF in treating BCa with LN metastasis. Further clinical studies are required for the application of targeting LINC00665 and HGF in LN metastatic BCa, presenting an encouraging prospect for broadening the application of blocking LINC00665 or HGF.

Previous studies have reported that RAB proteins are crucial mediators in endomembrane trafficking and modulating the budding efficiency of membrane-wrapped vesicles, thus widely participating in controlling the EV release [43, 44]. Moreover, the functional RABs also regulate the effect of EVs in their recipient cells during numerous biological events [45]. Yet, the knowledge about the vital regulator triggering the EV signaling in facilitating the LN metastasis of BCa is incomplete. Herein, through RNA-sequencing followed by the analysis of RAB expression patterns, we determined that RAB27B correlates specifically with LINC00665-driven lymphangiogenesis-associated EV secretion. We found that overexpression of RAB27B during the LN metastasis of BCa was caused by LINC00665-activated transcription of RAB27B, in which LINC00665 induced H3K4me3 modification on RAB27B promoter through recruiting hnRNPL. Moreover, RAB27B-induced EV secretion promoted CAF infiltration to stimulate BCa lymphangiogenesis and LN metastasis. These findings reveal the pivotal role of LINC00665-mediated RAB27B underlying lymphangiogenesis, deepening our understanding of RAB-mediated EV secretion in CAF-induced LN metastasis of BCa.

Recently, many biological molecules as potential therapeutic targets in BCa have been proposed, but most of them were hindered by their instability and biological barriers during the in vivo treatment [4]. Emerging evidences reveal that as crucial natural nanoscale vesicles, EVs exhibit an encouraging perspective in the molecular therapy of cancers due to their high histocompatibility and capacity for crossing biological barriers [17, 46]. Thus, it is of great importance to uncover the precise mechanism underlying the controlling of EV biogenesis and delivery. Here, we demonstrated that overexpression of lncRNA LINC00665 participated in the secretion of EVs that target fibroblasts. LINC00665 transcriptionally upregulated RAB27B to stimulate the secretion of EVs from BCa and endow EVs with a high affinity toward fibroblasts. Furthermore, silencing LINC00665 significantly impaired the targeted delivery of BCa cell-secreted EVs to fibroblasts and reduced CAF infiltration, which subsequently inhibited the lymphangiogenesis and LN metastasis of BCa in nude mouse popliteal LN metastasis model,

FIGURE 7 Clinical relevance of the LINC00665-induced RAB27B-HGF-c-Myc positive feedback loop in patients with BCa. (A and B) Representative images (A) and quantification (B) of LINC00665 expression, CAF infiltration, lymphatic vessel density, and HGF expression in BCa tissues. Scale bars: 50 μm. (C) Correlation analysis of LINC00665 and HGF expression in BCa tissues. (D and E) qRT-PCR analysis of HGF expression between BCa tissues and NATs ($n = 228$) (D) or between LN-negative ($n = 175$) and LN-positive ($n = 53$) BCa tissues (E). (F) Kaplan-Meier curves of the OS and DFS of patients with BCa with low *vs*. high HGF expression levels. The cutoff value is the median. (G) Representative bioluminescence images and quantification of popliteal metastatic LNs from nude mice treated with LINC00665-induced EVs with or without co-injection of αHGF ($n = 12$). Red arrows indicate footpad tumor and metastatic popliteal LN. (H) Representative images and quantification of IHC staining evaluation of LYVE-1-indicated lymphatic vessel density and α-SMA-indicated CAF infiltration in footpad tumors ($n = 12$). Red squares represent the areas of the insets. Scale bars: 50 μm. (I) Schematic illustration of the establishment of the PDX model. (J) Representative images and quantification of fluorescence of α-SMA-indicated CAFs and LYVE1-indicated lymphatic vessel density in PDX tumors from the mice ($n = 6$ per patient). Scale bar: 50 μm. (K and L) qRT-PCR analysis of LINC00665 expression in urinary EVs from patients with BCa ($n = 228$) and health control ($n = 228$), or BCa patients with ($n = 175$) or without ($n = 53$) LN metastasis. (M and N) ROC curves for the efficiency of urinary EV-mediated LINC00665 in diagnosing BCa and LN metastasis. (O) Proposed model of LINC00665-induced RAB27B-HGF-c-Myc positive feedback loop in promoting BCa lymphangiogenesis and LN metastasis. Statistical significance was assessed by the χ^2 test in B, the nonparametric Mann-Whitney *U* test in D, E, K and L, or 1-way ANOVA followed by Dunnett's tests in G-H. Error bars show the SD from three independent experiments. *$P < 0.05$; **$P < 0.01$. *Abbreviations*: BCa, bladder cancer; CAFs, Cancer-associated fibroblasts; qRT-PCR, quantitative real-time PCR; NATs, normal adjacent tissues; LN, lymph node; EVs, extracellular vesicles; OS, overall survival; DFS, disease-free survival; αHGF, neutralizing antibody against HGF; IHC, immunohistochemistry; LYVE-1, lymphatic vessel endothelial hyaluronan receptor 1; α-SMA, alpha-Smooth Muscle Actin; PDX, patient-derived xenograft; ROC, receiver operating characteristic analysis.

orthotopic xenograft model and PDX model. Our study suggested that LINC00665 could be an emerging technology target to modify and endow EVs with high targeting efficiency, which may provide a promising therapeutic strategy against the LN metastasis of BCa.

5 | CONCLUSIONS

In summary, we elucidate a novel mechanism underlying lncRNA-mediated EV secretion from BCa cells in facilitating the CAF-induced LN metastasis of BCa, in which the LINC00665-induced RAB27B-HGF-c-Myc positive feedback loop between tumor cells and fibroblasts sustains CAF infiltration and lymphangiogenesis. Our study highlights LINC00665-driven HGF signaling as a promising therapeutic target against tumor lymphangiogenesis and develops LINC00665 as a feasible sensitizer for anti-HGF treatment of LN metastatic BCa.

DECLARATIONS

AUTHOR CONTRIBUTIONS

Changhao Cheng and Jian Huang designed the study. Yuting Li, Hanhao Zheng, and Yao Kong performed the in vitro and in vivo experiments. Yan Lin, Yue Zhao and Mingjie An analyzed the clinical data. Yuting Li and Yan Lin carried out the ISH and IHC analysis. Yina Yin and Le Ai conducted the qRT-PCR and western blotting analysis. Yuming Luo, Yina Yin, Mingjie An and Yan Lin conducted the mechanistic experiments. Changhao Chen, Yuting Li, Yuming Luo, Yan Lin and Hanhao Zheng wrote the manuscript. All authors have read and approved the final manuscript, and the corresponding authors are responsible for all data, descriptions and aspects of this work. The order of the co-first authors was determined on the basis of their relative contributions.

ACKNOWLEDGMENT

We thank Yan Zhang and Xiaotao Cheng of Jizhi Medical Corporation, Suzhou, Jiangsu, P. R. China, for scRNA-seq personalized statistical consultation and Prof. Jinxin Zhang of the Department of Medical Statistics and Epidemiology, Sun Yat-Sen University, Guangzhou, Guangdong, P. R. China, for statistical advice and research comments.

FUNDING INFORMATION

This study was funded by the National Key Research and Development Program of China (Grant No. 2022YFA1305500 and 2018YFA0902803); the National Natural Science Foundation of China (Grant No. 82173272, 82173271, 81825016, 82103536, 82103416, 81871945 and 81902589); Guangdong Basic and Applied Basic Research Foundation (Grant No. 2021B1515020091, 2020A1515010815, 2018B010109006, and 2021A1515010355); and the Science and Technology Program of Guangzhou, China (Grant No. 202002030388, 201803010049, and 2017B020227007).

ETHICS APPROVAL AND CONSENT TO PARTICIPATE

All tissues and urine samples were obtained from patients who had undergone surgery at the Sun Yat-Sen Memorial Hospital of Sun Yat-Sen University with the consent of patients and the approval of the Sun Yat-Sen University Committees for Ethical Review of Research involving Human Subjects (approval number: 2013[61]). All animal experiments were performed with the approval of the Sun Yat-Sen University Institutional Animal Care and Use Committee (SYSEC-KY—KS-2021-293).

CONSENT FOR PUBLICATION

Not applicable

CONFLICT OF INTEREST STATEMENT

The authors declare no potential conflicts of interest.

DATA AVAILABILITY STATEMENT

More detailed methods are available in the Supplementary Materials and Methods. The data generated in the present study are available within the article and its supplementary data files. The sequence data generated in this study are publicly available in Gene Expression Omnibus (GEO) (RRID:SCR_005012) at GSE156308, GSE106534 and GSE190650. The scRNA-seq data were downloaded from EMBL-EBI datasets (https://www.ebi.ac.uk/ena/browser/view/PRJNA662018?show = reads, RRID:SCR_004727).

ORCID

Changhao Chen https://orcid.org/0000-0002-9924-9054

REFERENCES

1. Bray F, Ferlay J, Soerjomataram I, Siegel RL, Torre LA, Jemal A. Global cancer statistics 2018: GLOBOCAN estimates of incidence and mortality worldwide for 36 cancers in 185 countries. CA Cancer J Clin. 2018;68(6):394–424.
2. Bruins HM, Veskimae E, Hernandez V, Imamura M, Neuberger MM, Dahm P, et al. The impact of the extent of lymphadenectomy on oncologic outcomes in patients undergoing radical cystectomy for bladder cancer: a systematic review. Eur Urol. 2014;66(6):1065–77.
3. Lenis AT, Lec PM, Chamie K, Mshs MD. Bladder Cancer: A Review. JAMA. 2020;324(19):1980–91.
4. Cathomas R, Lorch A, Bruins HM, Comperat EM, Cowan NC, Efstathiou JA, et al. The 2021 Updated European Association

of Urology Guidelines on Metastatic Urothelial Carcinoma. Eur Urol. 2022;81(1):95–103.
5. Escobedo N, Oliver G. Lymphangiogenesis: Origin, Specification, and Cell Fate Determination. Annu Rev Cell Dev Biol. 2016;32:677–91.
6. Alitalo K, Carmeliet P. Molecular mechanisms of lymphangiogenesis in health and disease. Cancer Cell. 2002;1(3):219–27.
7. Su Y, Feng W, Shi J, Chen L, Huang J, Lin T. circRIP2 accelerates bladder cancer progression via miR-1305/Tgf-beta2/smad3 pathway. Mol Cancer. 2020;19(1):23.
8. Munir H, Mazzaglia C, Shields JD. Stromal regulation of tumor-associated lymphatics. Adv Drug Deliv Rev. 2020;161-162: 75–89.
9. Chen C, He W, Huang J, Wang B, Li H, Cai Q, et al. LNMAT1 promotes lymphatic metastasis of bladder cancer via CCL2 dependent macrophage recruitment. Nat Commun. 2018;9(1):3826.
10. Chen Y, McAndrews KM, Kalluri R. Clinical and therapeutic relevance of cancer-associated fibroblasts. Nat Rev Clin Oncol. 2021;18(12):792–804.
11. Bulle A, Lim KH. Beyond just a tight fortress: contribution of stroma to epithelial-mesenchymal transition in pancreatic cancer. Signal Transduct Target Ther. 2020;5(1):249.
12. Liu S, Chen X, Lin T. Lymphatic metastasis of bladder cancer: Molecular mechanisms, diagnosis and targeted therapy. Cancer Lett. 2021;505:13–23.
13. Mao X, Xu J, Wang W, Liang C, Hua J, Liu J, et al. Crosstalk between cancer-associated fibroblasts and immune cells in the tumor microenvironment: new findings and future perspectives. Mol Cancer. 2021;20(1):131.
14. Chen Z, Zhou L, Liu L, Hou Y, Xiong M, Yang Y, et al. Single-cell RNA sequencing highlights the role of inflammatory cancer-associated fibroblasts in bladder urothelial carcinoma. Nat Commun. 2020;11(1):5077.
15. Liu Y, Gu Y, Han Y, Zhang Q, Jiang Z, Zhang X, et al. Tumor Exosomal RNAs Promote Lung Pre-metastatic Niche Formation by Activating Alveolar Epithelial TLR3 to Recruit Neutrophils. Cancer Cell. 2016;30(2):243–56.
16. Zhang J, Ji C, Zhang H, Shi H, Mao F, Qian H, et al. Engineered neutrophil-derived exosome-like vesicles for targeted cancer therapy. Sci Adv. 2022;8(2):eabj8207.
17. Cheng L, Zhang X, Tang J, Lv Q, Liu J. Gene-engineered exosomes-thermosensitive liposomes hybrid nanovesicles by the blockade of CD47 signal for combined photothermal therapy and cancer immunotherapy. Biomaterials. 2021;275:120964.
18. Richter M, Vader P, Fuhrmann G. Approaches to surface engineering of extracellular vesicles. Adv Drug Deliv Rev. 2021;173:416–26.
19. Zhang WW, Wang QS, Yang Y, Zhou SY, Zhang P, Feng TB. The role of exosomal lncRNAs in cancer biology and clinical management. Exp Mol Med. 2021;53(11):1669–73.
20. Gong RQ, Nuh AM, Cao HS, Ma M. Roles of exosomes-derived lncRNAs in preeclampsia. Eur J Obstet Gynecol Reprod Biol. 2021;263:132–8.
21. Han M, Gu Y, Lu P, Li J, Cao H, Li X, et al. Exosome-mediated lncRNA AFAP1-AS1 promotes trastuzumab resistance through binding with AUF1 and activating ERBB2 translation. Mol Cancer. 2020;19(1):26.
22. Chen C, Luo Y, He W, Zhao Y, Kong Y, Liu H, et al. Exosomal long noncoding RNA LNMAT2 promotes lymphatic metastasis in bladder cancer. J Clin Invest. 2020;130(1):404–21.
23. Quail DF, Joyce JA. Microenvironmental regulation of tumor progression and metastasis. Nat Med. 2013;19(11):1423–37.
24. Zhan Y, Chen Z, Li Y, He A, He S, Gong Y, et al. Long non-coding RNA DANCR promotes malignant phenotypes of bladder cancer cells by modulating the miR-149/MSI2 axis as a ceRNA. J Exp Clin Cancer Res. 2018;37(1):273.
25. Zheng H, Chen C, Luo Y, Yu M, He W, An M, et al. Tumor-derived exosomal BCYRN1 activates WNT5A/VEGF-C/VEGFR3 feedforward loop to drive lymphatic metastasis of bladder cancer. Clin Transl Med. 2021;11(7):e497.
26. Chen C, Zheng H, Luo Y, Kong Y, An M, Li Y, et al. SUMOylation promotes extracellular vesicle-mediated transmission of lncRNA ELNAT1 and lymph node metastasis in bladder cancer. J Clin Invest. 2021;131(8):e146431.
27. Mathieu M, Martin-Jaular L, Lavieu G, Thery C. Specificities of secretion and uptake of exosomes and other extracellular vesicles for cell-to-cell communication. Nat Cell Biol. 2019;21(1):9–17.
28. Xu R, Rai A, Chen M, Suwakulsiri W, Greening DW, Simpson RJ. Extracellular vesicles in cancer - implications for future improvements in cancer care. Nat Rev Clin Oncol. 2018;15(10):617–38.
29. Zhu J, Luo Y, Zhao Y, Kong Y, Zheng H, Li Y, et al. circEHBP1 promotes lymphangiogenesis and lymphatic metastasis of bladder cancer via miR-130a-3p/TGFbetaR1/VEGF-D signaling. Mol Ther. 2021;29(5):1838–52.
30. Zhu Y, Xu G, Yang YT, Xu Z, Chen X, Shi B, et al. POSTAR2: deciphering the post-transcriptional regulatory logics. Nucleic Acids Res. 2019;47(D1):D203–D11.
31. Grote P, Herrmann BG. The long non-coding RNA Fendrr links epigenetic control mechanisms to gene regulatory networks in mammalian embryogenesis. RNA Biol. 2013;10(10):1579–85.
32. Atianand MK, Hu W, Satpathy AT, Shen Y, Ricci EP, Alvarez-Dominguez JR, et al. A Long Noncoding RNA lincRNA-EPS Acts as a Transcriptional Brake to Restrain Inflammation. Cell. 2016;165(7):1672–85.
33. Ostrowski M, Carmo NB, Krumeich S, Fanget I, Raposo G, Savina A, et al. Rab27a and Rab27b control different steps of the exosome secretion pathway. Nat Cell Biol. 2010;12(1):19–30; sup pp 1-13.
34. Jin H, Tang Y, Yang L, Peng X, Li B, Fan Q, et al. Rab GTPases: Central Coordinators of Membrane Trafficking in Cancer. Front Cell Dev Biol. 2021;9:648384.
35. Becker A, Thakur BK, Weiss JM, Kim HS, Peinado H, Lyden D. Extracellular Vesicles in Cancer: Cell-to-Cell Mediators of Metastasis. Cancer Cell. 2016;30(6):836–48.
36. Calon A, Tauriello DV, Batlle E. TGF-beta in CAF-mediated tumor growth and metastasis. Semin Cancer Biol. 2014;25: 15–22.
37. Biffi G, Tuveson DA. Diversity and Biology of Cancer-Associated Fibroblasts. Physiol Rev. 2021;101(1):147–76.
38. Sahai E, Astsaturov I, Cukierman E, DeNardo DG, Egeblad M, Evans RM, et al. A framework for advancing our understanding of cancer-associated fibroblasts. Nat Rev Cancer. 2020;20(3):174–86.

39. Gao X, Wan Z, Wei M, Dong Y, Zhao Y, Chen X, et al. Chronic myelogenous leukemia cells remodel the bone marrow niche via exosome-mediated transfer of miR-320. Theranostics. 2019;9(19):5642–56.
40. Hartmann S, Bhola NE, Grandis JR. HGF/Met Signaling in Head and Neck Cancer: Impact on the Tumor Microenvironment. Clin Cancer Res. 2016;22(16):4005–13.
41. Scagliotti GV, Novello S, von Pawel J. The emerging role of MET/HGF inhibitors in oncology. Cancer Treat Rev. 2013;39(7):793–801.
42. Zhang H, Deng T, Liu R, Bai M, Zhou L, Wang X, et al. Exosome-delivered EGFR regulates liver microenvironment to promote gastric cancer liver metastasis. Nat Commun. 2017;8:15016.
43. Colombo M, Raposo G, Thery C. Biogenesis, secretion, and intercellular interactions of exosomes and other extracellular vesicles. Annu Rev Cell Dev Biol. 2014;30:255–89.
44. Stenmark H. Rab GTPases as coordinators of vesicle traffic. Nat Rev Mol Cell Biol. 2009;10(8):513–25.
45. Wang FW, Cao CH, Han K, Zhao YX, Cai MY, Xiang ZC, et al. APC-activated long noncoding RNA inhibits colorectal carcinoma pathogenesis through reduction of exosome production. J Clin Invest. 2019;129(2):727–43.
46. Wang H, Alarcon CN, Liu B, Watson F, Searles S, Lee CK, et al. Genetically engineered and enucleated human mesenchymal stromal cells for the targeted delivery of therapeutics to diseased tissue. Nat Biomed Eng. 2021.

SUPPORTING INFORMATION

Additional supporting information can be found online in the Supporting Information section at the end of this article.

How to cite this article: Li Y, Zheng H, Luo Y, Lin Y, An M, Kong Y, et al. An HGF-dependent positive feedback loop between bladder cancer cells and fibroblasts mediates lymphangiogenesis and lymphatic metastasis. Cancer Commun. 2023;1–23. https://doi.org/10.1002/cac2.12470